From the: ***Walther-Straub-Institute for Pharmacology and Toxicology***
of the Ludwig-Maximilians-University Munich

Dissertation

zum Erwerb des Doctor of Philosophy (Ph.D.) an der

Medizinischen Fakultät der

Ludwig-Maximilians-Universität zu München

TRP Channels in Pulmonary Disease & Lung Toxicology

vorgelegt von:

Christian Volker Schremmer

aus:

Fulda, Germany

Jahr:

2023

Mit Genehmigung der Medizinischen Fakultät der

Ludwig-Maximilians-Universität zu München

First supervisor: Prof. Dr. Alexander Dietrich

Second supervisor: Prof. Dr. Annette Nicke

Third supervisor: PD Dr. Claudia Staab-Weijnitz

Dean: **Prof. Dr. med. Thomas Gudermann**

Datum der Verteidigung:

27.07.2023

Affidavit

Affidavit

Schremmer, Christian

Surname, first name

Street

Zip code, town, country

I hereby declare, that the submitted thesis entitled:

TRP Channels in Pulmonary Disease & Lung Toxicology

……

is my own work. I have only used the sources indicated and have not made unauthorized use of services of a third party. Where the work of others has been quoted or reproduced, the source is always given.

I further declare that the submitted thesis or parts thereof have not been presented as part of an examination degree to any other university.

Munich, 28.03.2022

place, date

Christian Schremmer

Signature doctoral candidate

Confirmation of congruency

LMU LUDWIG-MAXIMILIANS-UNIVERSITÄT MÜNCHEN

Promotionsbüro
Medizinische Fakultät

MMRS

Confirmation of congruency between printed and electronic version of the doctoral thesis

Schremmer, Christian

Surname, first name

Street

Zip code, town, country

I hereby declare, that the submitted thesis entitled:

TRP Channels in Pulmonary Disease & Lung Toxicology

……

is congruent with the printed version both in content and format.

Munich, 28.03.2022

place, date

Christian Schremmer

Signature doctoral candidate

Table of content

List of abbreviations

2D	Two dimensional
3D	Three dimensional
ALI	Acute Lung Injury
ALI	Air Liquid Interface
AQP-5	Aquaporin 5
ARDS	Acute Respiratory Distress Syndrome
ANKs	Ankyrin-repeat domains
AT1/2	Alveolar Type 1/2
BMEL	German Federal Ministry of Food and Agriculture
CAST	Computer Assisted Stereological Toolbox
CaM	Calmodulin-binding domain
CBF	Ciliary Beat Frequency
CIRB domain	Calmodulin and IP3 Receptor Binding domain
COPD	Chronic Obstructive Pulmonary
CoV2	Corona Virus 2
CPFE	Combined Pulmonary Fibrosis and Emphysema
C-terminal	Carboxy-terminal
DAG	Diacylglycerol
ECM	Extracellular Matrix
FITC	Fluorescein Isothiocyanate
GFP	Green Fluorescent Protein
HEK	Human Embryonic Kidney cells
ip	Intraperitoneally
IPF	Idiopathic Fibrosis
IPVML	Isolated Perfused and Ventilated Murine Lung
IRES	Internal Ribosome Entry Site
IR-induced	Ischemia-Reperfusion- induced
iv	Intravenously
KO	Knockout
MCL	Mean Chord Length
N-terminal	Amino-terminal
PBD	Phosphoinositide Binding Domain
PBS	Phosphate-Buffered Saline
PDMS	Poly(dimethylsiloxane)
PFA	Paraformaldehyde
PLC	Phospholipase C
SARS	Severe Acute Respiratory Syndrome
SP-A/-B/-C/-D	Surfactant Protein A/-B/-C/-D
TRPA channel	Ankyrin Transient Receptor Potential channel
TRPC channel	Classical Transient Receptor Potential channel
TRPM channel	Melastatin Transient Receptor Potential channel
TRPV channel	Vanilliod Transient Receptor Potential channel
VILI	Ventilator-induced Lung Injury
WT	Wild type

List of publications

Research paper I:

Weber, J., Rajan, S., Schremmer, C., Chao, Y., Krasteva-Christ, G., Kannler, M., Yildirim, A. Ö., Brosien, M., Schredelseker, J., Weissmann, N., Grimm, C., Gudermann, T., Dietrich, A. TRPV4 channels are essential for alveolar epithelial barrier function as protection from lung edema. *JCI Insight* **20**, e134464 (2020). https://doi.org/10.1172/jci.insight.134464

Research paper II:

Schremmer, C., Steinritz, D., Gudermann, T., Beech, D. J., Dietrich, A. An *ex vivo* perfused ventilated murine lung model suggests lack of acute pulmonary toxicity of the potential novel anticancer agent (−)-englerin A. *Arch Toxicol* **96**, 1055–1063 (2022). https://doi.org/10.1007/s00204-022-03235-z

Review:

Rajan, S., Schremmer, C., Weber, J., Alt, P., Geiger, F., Dietrich, A. Ca^{2+} Signaling by TRPV4 Channels in Respiratory Function and Disease. *Cells* **10**, 822 (2021). https://doi.org/10.3390/cells10040822

Contribution to the publications

1.1 Contribution to Research paper I

Next to providing a critical analysis and revising the manuscript, my primary contribution as a shared second co-author of the first publication included the implementation and analysis of immuno-histochemical experiments with paraffin-embedded lungs. According to the advice by one reviewer of the revision process, the first set of paraffin-embedded lung sections, which had been treated with paraformaldehyde (PFA) for fixation, had to be reevaluated. Already analyzed and new additional tissue samples for each time point had to be processed and evaluated again. This preparation included perfusion and inflation of lungs with 2,5% (m/v) glutaraldehyde in phosphate-buffered saline (PBS), processing for paraffin embedding, sectioning, mounting on glass slides and staining with Masson Goldner trichrome dye. Mean chord lengths (MCL) were analyzed in tissue sections by design-based stereology using an Olympus BX51 light microscope equipped with the new Computer Assisted Stereological Toolbox (newCAST, Visiopharm) at the Helmholtz Institute lab of Dr. Ali Önder Yildirim. In this setup, mice with (wild type, WT) and without (TRPV4-/-, KO) functional TRPV4 channels were compared in three age groups: young (4-6 weeks of age), middle-aged (28-30 weeks of age) and old (47-52 weeks of age) mice of both sexes (see figure 6 of this publication). Elevated mean chord length values in old TRPV4-/- mice compared to same aged WT mice as well as representative images confirmed the development of emphysema-like changes due to ongoing growth and repair processes in accordance with previous gathered data of altered lung function in adult TRPV4-/- mice.

1.2 Contribution to Research paper II

I conducted the experimental setup, data acquisition and analysis as well as contributed to the first draft of the manuscript and the revision as the first author of the publication. Specifically, the setup for toxicant induced pulmonary edema formation in the isolated, perfused and ventilated murine lung (IPVML) system had to be established. While the development of ischemia-reperfusion (IR)-induced pulmonary edema quantified in the first publication relied upon a stop of perfusion for a certain amount of time a new experimental protocol and construction for the controlled addition of toxicants or solvents to the perfusion had to be established for the toxicant-induced edema setup. A robust positive control for edema formation by short-time pH drops was implemented and a dose-response relationship was confirmed after analysis of different parameters of the IPVML setup and wet-to-dry weight ratios.

(-) Englerin A was chosen as a drug to be tested and dissolved in a Novartis approved standard solution for all in-life preclinical evaluations. It had to be demonstrated that both the Novartis standard solution itself did not increase the risk of pulmonary edema formation in the IPVML setup and that (-) Englerin A, as a substance, was active in the chosen concentrations in the perfusion solution. To confirm biological activity of the selected concentrations of (-) Englerin A in the IPVML setup Ca^{2+} imaging experiments with HEK293T cells transfected with a TRPC4β1 cDNA in a pIRES2 plasmid containing an eGFP cDNA under the control of the internal ribosome entry site (IRES) and mock transfected control cells were performed. Results showed a completely preserved biological activity of the chosen concentrations of (-) Englerin A in perfusion solutions after one hour of perfusion in the IPVML.

Moreover, a protocol for the permeation of fluorescein isothiocyanate (FITC)-coupled dextran particles was established in *ex vivo* lungs. Perfused lungs were cut into cryosections and analyzed using both a confocal microscope and a fluorescence slide scanner. With this protocol a dose-response relation between tissue permeation and short-time pH drop was demonstrated and compared to perfusion with (-) Englerin A, which did not show a significant increase for incorporation of FITC-dextran particles similar to the solution-only perfused mouse lungs. In a final step, data analysis was performed using a self-written script in R and graphs were prepared using GraphPad Prism 9.

2. Introduction

2.1 Cells and Functions of the Respiratory System

The respiratory system is one of the few organs in the human body, next to the skin, that is in permanent contact with the environment. Xenobiotics and pathogens are in close proximity to the huge volume of the respiratory system, with one of the narrowest borders found in organisms and most permeable epithelial barrier of the human body [1]. The whole system can be divided into the upper, conducting airways and the lower, respiratory airways. The conducting airways consist of the nasal cavity, pharynx, larynx, trachea and upper bronchi. Following the bifurcation of the trachea into the two primary bronchi, they continue to branch forming first lobar, then segmental bronchi, bronchioles, and finally terminal bronchioles [2]. The terminal bronchioles mark the transition from conducting into respiratory airways, with respiratory bronchioles leading into the alveolar duct and alveolar sac, where the main gas exchange takes place. In the conducting airways, the pseudostratified epithelium of mucus producing goblet cells and ciliated cells is responsible for mucociliary clearance as a first mechanism of defense. Club cells produce surfactant proteins with antimicrobial properties, whereas basal cells act as progenitor cells in the process of repair and replacement. In more distal parts of the bronchi, the pulmonary epithelium flattens and grows thinner with the amount of ciliated cells decreasing, while numbers of club cells are increasing. Finally, the epithelial membrane of respiratory bronchioles and alveoli consists predominantly of pneumocytes [2, 3].

In the respiratory airways, there are two types of pneumocytes: the long, stretched and squamous Alveolar Type 1 (AT1) cells and the cubical shaped Alveolar Type 2 (AT2) cells, which build up the delicate pulmonary membrane that facilitates gas exchange in close proximity to endothelial cells of the alveolar capillaries. Because of their flat shape, AT1 cells compose up to 95-98% of the alveolar surface, but are far outnumbered by AT2 cells, which make up more than 60% of the cell count [4, 5]. The approximated diameter of just 2 - 0,2 µm of alveolar-epithelial membranes is the main reason for the efficient gas exchange, but on the flipside makes it one of, if not the most vulnerable, spots in the human organism. AT1 cells are highly water permeable and, therefore, are central for ion transport and fluid homeostasis with the help of water conducting aquaporin 5 (AQP-5) channels, which are the only isoform found in alveolar cells [6, 7]. Next to playing a role in ion transport and fluid homeostasis, AT2 cells act as progenitor cells in repair and renewal processes in the lung. They not only produce and secrete surfactant proteins, mainly surfactant protein C (SP-C), but also are responsible for recycling and storage.

SP-C, as other isoforms (A, B & D), is essential for various processes in the respiratory system. SP-C from AT2 cells notably reduces surface tension in the alveoli and, therefore, the pulmonary compliance, a value for the ability to stretch and expand [3]. Surfactants, in general, are essential to prevent alveolar collapse and help to restore already collapsed alveoli. A defect in surfactant production can lead to a breakdown of alveolar structure and emphysema-like structures resulting, if not treated properly, in a

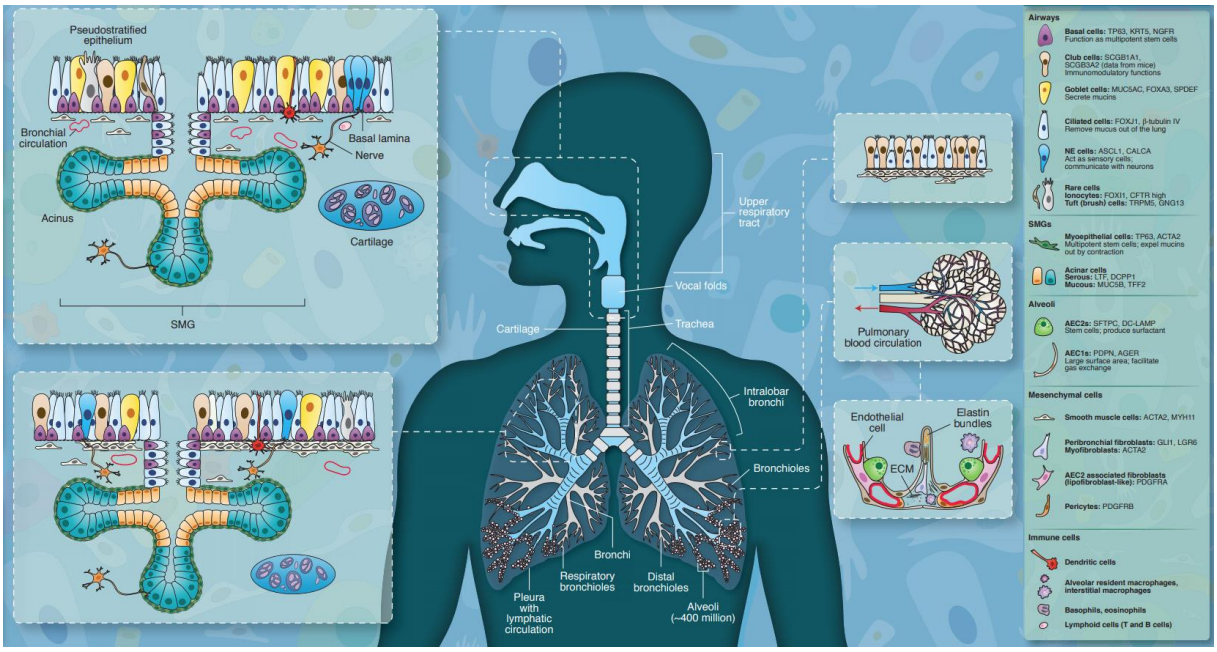

Figure 1: The respiratory system. Cellular composition and organization of conducting & respiratory airways, summary of the different cell types (right). See text for further details. Modified after [2].

complete loss of breathing capacity [8, 9]. In addition, SP-A and SP-D are secreted by club cells in the upper airways and have antimicrobial properties as well [10]. In addition to pneumocytes, the alveolar space is populated by alveolar macrophages as well. The phagocytic macrophages are essential for the immune response and clearing of the lung from harmful particles and microorganisms impairing the gas exchange.

Even before the outbreak of the COVID-19, pandemic diseases of the respiratory system were among the three major causes of death around the globe in 2019 [11]. The development of edema is a common comorbidity for most pulmonary diseases like chronic obstructive pulmonary disease (COPD), infections of the lower respiratory tract, acute lung injury (ALI) or the acute respiratory distress syndrome (ARDS). In particular, the mortality in patients suffering from severe acute respiratory syndrome coronavirus 2 (SARS-CoV-2) infection is driven by pulmonary edema formation [12]. The development of acute pulmonary edema is a medical emergency and life threatening condition [13], and will be described in more details in the following chapter.

2.2 Lung Damages

Acute pulmonary edema formation is defined as sudden fluid accumulation in the lung, a life-threatening condition and medical emergency. Edema formation is the result of a failed mechanism of removal of fluid invading the pulmonary interstitium and alveoli [14]. In a regular healthy lung, the homeostasis between blood flow and breathing pattern is tightly regulated to provide a sufficient gas exchange. Under normal conditions, fluids from the capillaries can be transferred to the interstitium through gaps between the endothelial cells, but are restricted from entering the alveolar space due to very tight junctions of the epithelial barrier. Even if fluids enter the alveolar space, they can be removed by simultaneous active transport of ions into the interstitium by

Na^+/K^+ - ATPases and fluids by aquaporins followed by lymphatic drainage. In a simplified approach, acute pulmonary edema can be classified as either cardiogenic or non-cardiogenic edema [15].

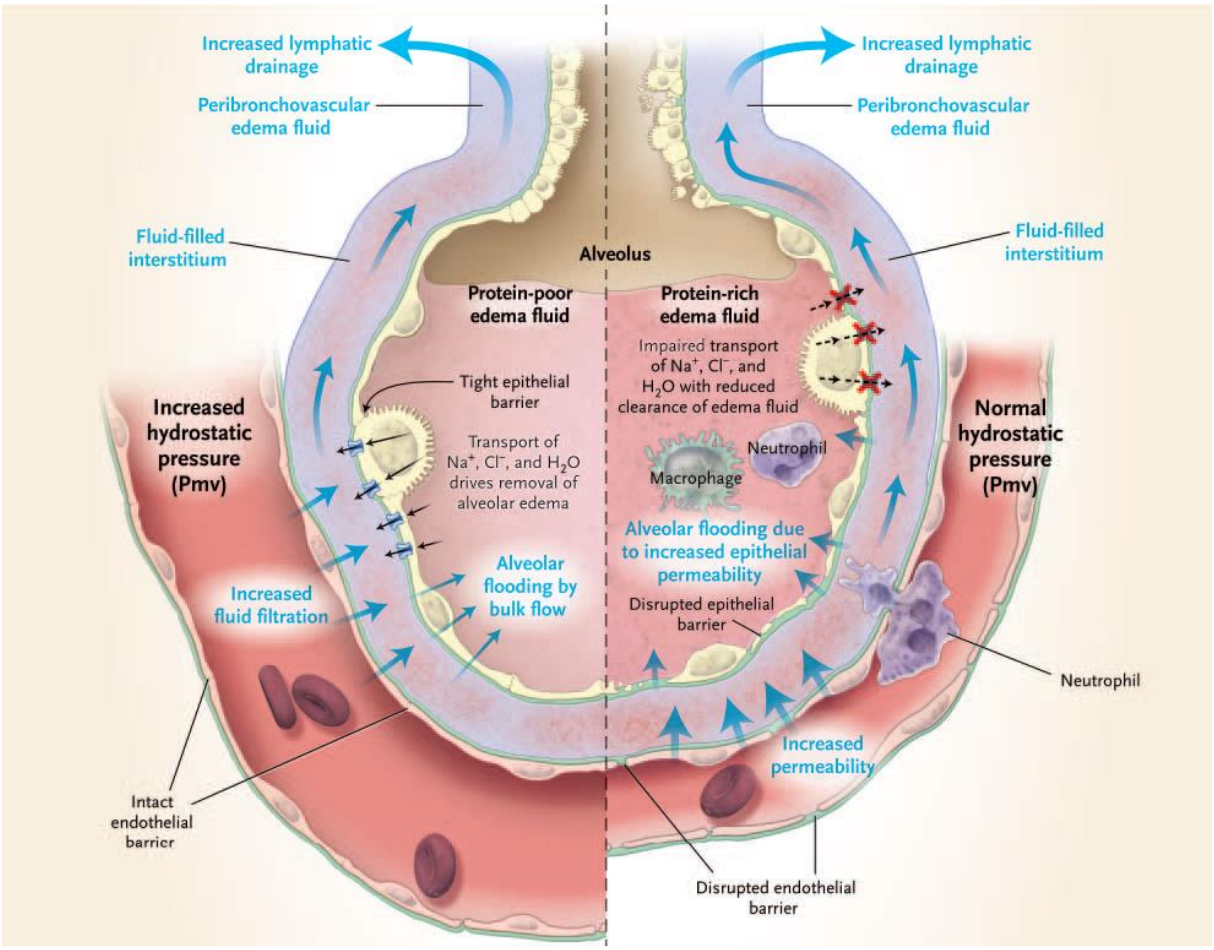

Figure 2: Pulmonary edema formation. Physiological differences in the formation of cardiogenic (left) & non-cardiogenic (right) edema. See text for further details. Modified after [15].

2.2.1 Cardiogenic edema

During classic cardiogenic edema formation, increased hydrostatic pressure leads to an increased fluid filtration at the endothelial barrier between the vasculature and the pulmonary interstitium. If this increase can not be compensated by an increase in lymphatic drainage, the alveolar space is flooded by a bulk flow. Because proteins are filtered by the still intact endothelial barrier, the edema fluid stays protein-poor [16]. This type of edema formation usually is a result of left-sided heart failure, a condition in which the muscle of the left ventricle is weakened and fails to deliver oxygen rich blood from the lung to the vital organs of the body. Common causes include heart related diseases such as myocardial infarctions, coronary artery disease and cardiomyopathy. As a result, a congestion of fluids in the pulmonary circulation occurs [17, 18].

2.2.2 Non-Cardiogenic Edema

In contrast to cardiogenic edema, non-cardiogenic edema is caused by an increase in permeability of the endothelial and/or epithelial barrier. In both cases, alveoli are filled with edema fluid at a normal hydrostatic pressure. Increased permeability at the endothelial barrier causes an increase of fluid transported to the alveolar interstitium. If not cleared by increased lymphatic drainage, this fluid transport leads to alveolar flooding by increased permeability of the epithelial barrier. In contrast to cardiogenic edema formation, the fluid now contains more protein due to missing filtration by the endothelial barrier. The transport of ions and water is impaired, resulting in reduced clearance. The amount of fluid and severity of the edema formation depends on one or both barriers and the degree of injury. In ALI/ARDS patients, severe inflammatory processes increase the permeability due to damage in alveolar epithelial cells and reduced vascular endothelial barrier function. Infiltration and activation of neutrophils exacerbates lung injuries. Initial wound repair processes involve fibrotic and neovascular processes and often overlap with the acute edema phase. Usually, mechanical ventilation is the first intervention. However, recent studies, particularly with focus on the treatment of COVID-19 patients, demonstrated that ventilation itself not only aggravates but initiates lung injuries (ventilator-induced lung injury (VILI)) [19, 20]. Once edema fluids fill the alveolar space, the effect of surfactants is impaired and surface tension increases. Sudden flooding of the interstitium and the resulting increase in pressure on the epithelial membrane can result in lesions and mechanical injuries. The disruption of the epithelial barrier is associated with pulmonary capillary stress failure and acute lung injuries, followed up by inflammation.

2.2.3 Risk factors

Certain comorbidities such as hypertension, diabetes and smoking favor edema formation [17]. Smoking is a major cause in the development of COPD and pulmonary emphysema, a common morbidity characterized by the destruction of alveolar structure and resulting in enlarged air-filled spaces in the lower lung. The amount of destruction correlates with the expansion of alveoli and is measured in mean alveolar width or mean chord length (MCL). The outcome of an excessive expansion of emphysema is a reduced alveolar surface and impaired gas exchange, as well as an increased risk for alveolar collapse. Additionally, patients suffering from COPD and emphysema are prone to an increased edema formation. A potential amplifying effect between pulmonary emphysema and idiopathic fibrosis (IPF) for diseases like combined pulmonary fibrosis and emphysema (CPFE) is in discussion [21, 22].

2.3 TRP Channels

For the development of pulmonary edema, ion channels in the plasma membranes, like the non-selective transient receptor potential (TRP) channels, are also of outmost importance. These channels may act as sensors for different physical and chemical stimuli and are also involved in the progression of pulmonary disease like COPD, asthma, pulmonary fibrosis and edema [23-26]. If triggered by toxicants, these channels could increase microvascular permeability in the lung and increase the risk for edema formation [27]. Recently, TRP channels were even proposed as potential target for the treatment of COVID-19 associated diseases and the prevention of side effects

of other drugs [12, 28, 29]. The superfamily of transient receptor potential (TRP) channels in mammals consists of 28 mostly nonselective cation channels with major permeability for Na^+, Ca^{2+} and Mg^{2+} ions. These TRP channels, which can be divided into 6 families, are located in the plasma membrane of almost every tissue and play a major role in signaling cascades for Ca^{2+} homeostasis [30, 31]. TRP channels share a common segment of six transmembrane domains with a pore-forming region between the fifth and sixth domain as well as intracellular amino- (N) and carboxy (C)-terminal domains, which vary between the subgroups in both length and structure. The so-called TRP-box, found only in the C-terminal region of TRPC , TRPV and TRPM channels, is one of the highest conserved regions in the TRP channel superfamily [32] and may play a role in membrane localization and opening of the channel [33, 34]. Another common structure for TRP channels are ankyrin-repeat-domains (ANKs) at the N-terminus found in members of the TRPC, TRPV and TRPA channel families, with the highest number of 14 ANKs in the TRPA1 channel. These repeats are involved in protein-protein interaction, may help in the formation of functional tetrameric channels at the plasma membrane and could potentially bind small molecules [35, 36].

2.3.1 Vanilloid TRP (TRPV) Channels and TRPV4

The vanilloid subfamily of TRP channels (TRPV) was first discovered in 1997 as target receptor for capsaicin, an irritant alkaloid metabolite found in chili peppers that provides the sensation of heat and pain when ingested, inhaled or just in case of skin contact [37]. Unique characteristics of TRPV channels are up to six N-terminal ankyrin-repeat domains followed by a phosphoinositide binding domain (PBD) important for plasma membrane localization, a C-terminal calmodulin-binding domain (CaM), and a PDZ-binding-like motif [38]. Since the first discovery of TRPV1 described in 2020, the subgroup of TRPV channels has grown to six members in total, subdivided into two groups. TRPV1-4 are non-selective cation channels whereas TRPV5 & 6 are selective for Ca^{2+} with important functions in the Ca^{2+} homeostasis of the intestine and kidneys [39].

TRPV4 is expressed almost ubiquitously in the body including in many cells of the respiratory system. Expression has been confirmed in tracheal [40] and bronchial cells [41] of the upper respiratory tract and in epithelial and endothelial cells of the alveolar tract [42, 43], as well as in various immune cells [44, 45]. The functional TRPV4 channels consist of four channels forming a homotetrameric complex, with increased permeability for Ca^{2+} and Mg^{2+} ions compared to Na^+ ions [46]. TRPV4 is thermosensitive and can be activated by shear stress, changes in osmolality and pressure [38]. Because of their extensive expression in the respiratory system and versatile mechanisms of activation, TRPV4 channels are involved simultaneously in both defensive and harmful mechanisms. In tracheal epithelial cells, TRPV4 is suggested to be expressed predominantly in cilia regulating ciliary beat frequencies (CBF). As a translator of physiological stimuli into cellular signals, TRPV4 plays a key role in mucociliary clearance and host defense [47]. Recently, Scheraga et al. demonstrated a protecting effect of TRPV4 in macrophages against bacterial pneumonia [48].

The expression of TRPV4 in pulmonary endothelial cells makes it particularly interesting as a potential target in the development of pulmonary edema. TRPV4 channels are involved in endothelial transcytosis, the active transport of cellular compounds across

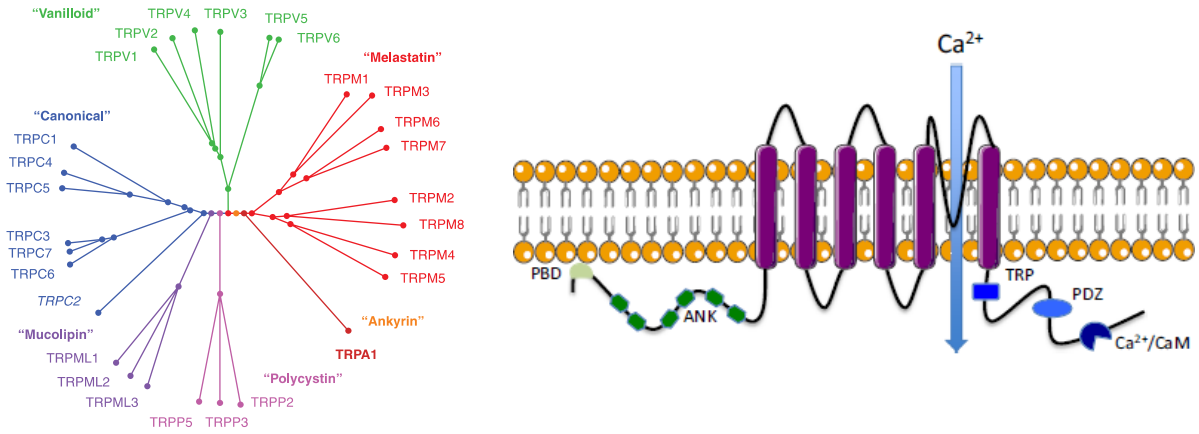

Figure 3: The TRP channel superfamily. Members of the mammalian TRP channel superfamily (left) and schematic presentation of the TRPV4 channel (right). Phosphoinositide Binding Domain (PBD); Ankyrin-repeat domain (ANK); TRP-box domain (TRP); PDZ-binding-like motif (PDZ); Calmodulin-binding domain (CaM).See text for further details. Modified after [31] and [38].

a membrane, through the interior of cells [49]. In combination with its role as a mechanosensor, TRPV4 plays a central role in endothelial permeability and barrier structure. Activation of TRPV4 has been linked to increased pulmonary vascular permeability and Ca^{2+} influx-mediated barrier failure [50].

However, it is still elusive whether only TRPV4 mediated Ca^{2+} influx or a resulting activation of voltage gated Ca^{2+} channels triggers these effects [51]. Experiments with TRPV4 deficient mice suggest a direct effect of TRPV4 in endothelial cells on barrier function, as these mice were protected from ALI after acid installation [52]. The inhibition of TRPV4 channels was proven to be an effective treatment for chemically induced acute lung injuries. Mice after inhalation or intratracheal administration of toxic gasses, like chlorine and acidic compounds, suffer from hyperreactive airways as well as pulmonary and systemic inflammation usually followed by acute lung injury and edema formation. These symptoms are reduced for both mice with a TRPV4 deficiency and mice treated with TRPV4 antagonist following the exposure [53, 54]. In the treatment of lung injuries after inhalation of phosgene, a highly reactive and toxic gas used as chemical warfare agent in world war I, TRPV4 inhibition is suggested to reduce edema formation and improve survival rates [55].Other possible roles of TRPV4 channels in lung epithelial cells, however, are still elusive.

2.3.2 Classical TRP (TRPC) Channels and TRPC4

The family of canonical transient receptor potential channels (TRPC) consists of seven members which can be further divided into three structural homologous subgroups TRPC1/TRPC4/TRPC5, TRPC3/TRPC5/TRPC7 and TRPC2. All these channels are non-selective cation channels with 3-4 N-terminal ankyrin-repeats, coiled-coil domains as well as a calmodulin and IP3-receptor binding (CIRB) domain. All members of the TRPC family may form functional tetrameric channels except for TRPC1, which may act more as a channel regulator than an ion channel itself [56, 57]. All TRPC channels are activated by ligand-bound receptors, which stimulate phospholipase C

(PLC) to produce diacylglycerol (DAG). TRPC channels are expressed in many different organs in the body, primarily in cells of the central nervous system, and act as sensors for temperature, pain and other stimuli [58]. Activation of heteromeric TRPC4/TRPC1 channels was demonstrated to have cytotoxic effects in synovial sarcoma cells and inhibit tumor growth, which makes the channels interesting as targets for potential anti-cancer drugs [59]. For (-) Englerin A, an anticancer drug candidate with a high potential against kidney cancer, its activation of TRPC4/5 would not only induce a cytotoxic effect in cancer cells but also an increase in vascular permeability and a potential risk for pulmonary edema formation [27, 60]. The investigation of this effect is complicated, however, by the inadequacies of existing *in vivo* toxicology models [61].

2.4 Experimental Models in Lung Disease and Toxicity

As outlined above, the role of TRP channels in the (patho-) physiology of the lung is of particular interest. Suitable *in vivo* and *in vitro* models are needed to dissect their roles in lung disease and toxicity and to identify them as potential therapeutic targets. As every *in vivo*, *ex vivo* and *in vitro* lung model has its own advantages and disadvantages, there is not a single experimental system suitable for answering all questions. This chapter contains an overview and description of the available models.

Since the invention of animal testing in the 19th century, the advantages and disadvantages for animal experimentation in the evaluation of new drugs have been discussed extensively. As animal experiments are still essential in the evaluation of physiological processes, therapeutic monitoring, drug delivery and safety, research on adverse health effects on animals has significantly improved their welfare. Russel and Burch published “The Principle of Human Experimental Technique” in 1959 and established the 3R principles (replacement, reduction, refinement) for animal testing. They propose, in brief, if animal testing can not be replaced by state-of-the-art *in vitro* cellular experiments, remaining animal numbers must be reduced and conditions for animal testing need to be refined. Two dimensional (2D) *in vitro* (primary) cell culture models and *ex vivo* 3D cell culture models are continuously becoming more developed and refined, and may partly replace animal experiments in the near future. With a focus on the pharmacology and toxicology of the lung, different novel approaches will be discussed in the following paragraphs.

2.4.1 *In Vivo* Models

One possible approach in mimicking the human pulmonary system is using closely related *in vivo* animal models as substitutes. In a report by the German Federal Ministry of Food and Agriculture (BMEL), the amount of animals used in Germany for scientific purposes is estimated at about 2,8 million, of which about 2,1 million have been used in animal experiments in 2019. Since the use of human and non-human primates in drug testing is banned for ethical reasons, small animals with high reproductive rates are the first choice. Murine animals make up the largest portion of experimental organisms, followed by fish [62].

As far as comparability with clinical trials on human subjects is concerned, *in vivo* animal models are heavily favored over existing cellular models. With a focus on lung

toxicology, so far no cellular setup manages to imitate the structure and complex interactions of the heart and lung, endothelial and epithelial barrier, breathing and blood flow. Breeding patterns and gene silencing techniques enable the comparison of different genotypes in development, phenotypic expression and response to toxicants in both acute and chronic interactions.

On the downside, the use of animals always brings a high variability of different species into account. Next to intra- and interspecies variability, the conditions in which the animals are kept, differences in the experimental procedure as well as the type of application of drugs is of utmost importance. If injected intraperitoneally (ip) or intravenously (iv), uneven distribution of an experimental compound can be problematic, especially if the alveolar space is targeted. Injection into the nasal cavities might overcome this problem, but induces even more stress in the animal, which can alter behavior and might affect metabolism [63]. Stress in animals causes a difference in heart rate and breathing pattern that can alter the exposure of the animal and therefore the final concentration that reaches the lung. One way to overcome these issues is to employ a special breathing chamber that allows ventilated exposure of animals to modified mixtures of air, toxic gasses or dusts.

2.4.2 *In Vitro* Models

In vitro model systems rely on primary cells, dissected from treated or modified individuals, or immortalized cell lines cultured outside their usual biological environment on standardized cell culture dishes. These models are essential for initial drug evaluation, dose-response relationships and the molecular mechanism and physiological effects of exposure to target substances. They stand out with a straightforward approach and reduction of interactions compared to organs or multicellular organisms. *In vitro* models can be used for in depth studies of biochemical functions and for obtaining initial data about the pharmacology and toxicology of a drug. Despite this reduction, data obtained in *in vitro* models are versatile; data acquisition is highly standardized and provides the opportunity for high-throughput screenings [64]. In lung toxicology, regular 2D cell culture monolayers of respiratory epithelial cells are used for first hand cytotoxicity testing, growth, viability and differentiation assays. Especially the differentiation of pulmonary pneumocytes under different conditions, their viability and molecular signaling after exposure to toxicants can be studied in these setups. The co-cultivation of different cell types reduces some restrictions of conventional monolayer models. Epithelial cells grown in air liquid interface (ALI) cultures differentiate into functional epithelial tissue. Progenitor cells grown in 3D cell culture models can differentiate and organize into organoids.

In a next step, these miniaturized organs can be grown on microchips equipped with microfluidic systems for more precise and lifelike supply of water and nutrients [65]. Microfluidic systems are devices containing small (10-100 µm in diameter) channels to manipulate and process small (µl-nl) amounts of liquids [66, 67]. In a first attempt combining *in vitro* cell culture with microfluidic system, Huh et al. in 2010 grew endothelial and epithelial cells on both sides of a porous and flexible poly(dimethylsiloxane) (PDMS) membrane [48]. Air-liquid interface cell culture, which can easily manipulated by mechanical forces on the air side, can be combined with nutrient exchange, by a

dynamic flow through the microfluidic system on the other side, to create the first alveolar-capillary surrogate. Nowadays, lung-on-a-chip models are utilized in lung toxicology [68, 69], asthma [70] and to investigate a better strategy and dosage for chemotherapy [71]. Co-culturing of cell types in combination with a microfluidic system may be able to mimic different types of human organs.

Yet, one main disadvantage of cell culture systems is a questionable extrapolation from cultured cells to the complete organism. Lung-on-a-chip models have to be designed specifically for the experimental setup, and current materials are still far from replacing the natural endothelial-epithelial barrier in both morphology and toxicological potential [72].

2.4.3 The Isolated, Perfused and Ventilated Murine Lung (IPVML) Model

The concept of studying the physiology and biochemistry of the lung *ex vivo* was developed in the 1970s. Initial, less sophisticated approaches were limited to the use of rat lungs for perfusion and drug metabolism studies. Conversion of compounds after perfusion through the lung, arterial pressure and weight could be monitored as well as alterations in tissue histology and the formation of edema. Until the early 1990s, these systems usually relied on a positive pressure ventilation and did not include the evaluation of gas exchange and lung breathing mechanics [73].

Uhlig and Wollin in cooperation with Hugo Sachs Electronics where the first to describe a setup for ventilating rat lungs with negative pressure and simultaneous monitoring of the lung weight [74]. Ventilating lungs with a negative pressure is not only less harmful and less prone to unintended edema formation, but is also closer to the *in vivo* situation with the possibility to add deep inhalations as hyperinflations to preserve elasticity and extensibility in the *ex vivo* setup. Nowadays, advances in the setup allow the use of much smaller mouse lungs from genetically modified animals [75, 76]. Modern software and components pave the way for more precise and robust data acquisition and processing.

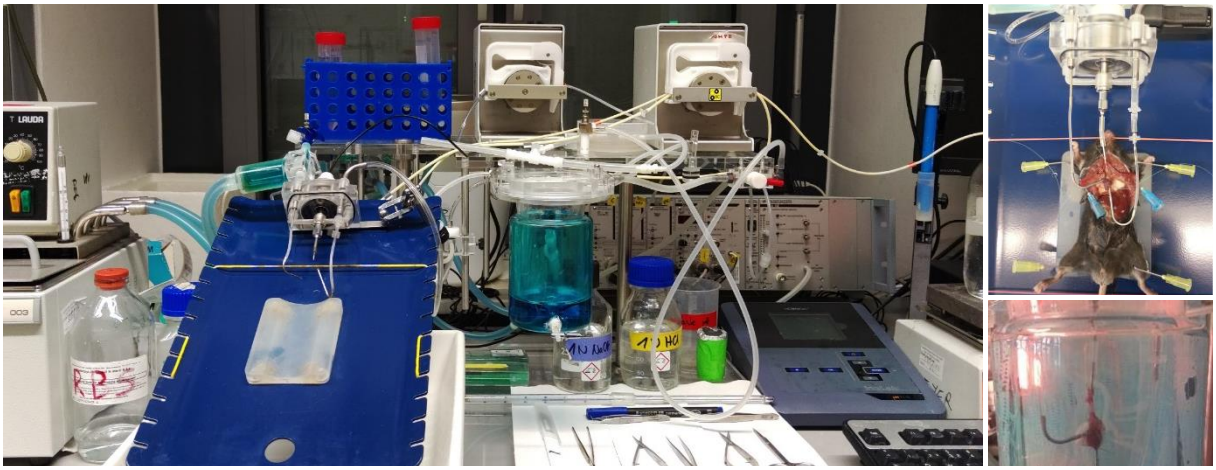

Figure 4: The Isolated Perfused and Ventilated Murine Lung (IPVML) model. Total view of the IPVML model used in this thesis (left). Example picture of a successful preparation with cannulas installed in the trachea, the pulmonary artery and the left ventricle (upper right). Dissected heart & lung in the artificial thorax, perfused with electrolyte solution.

Compared to the animal models described above, the isolated perfused and ventilated murine lung (IPVML) system has its unique advantages. As in common *in vivo* rodent models, lung and heart are utilized as a physiological unit. The intact perfusion and ventilation *ex vivo* inside an artificial thorax mimics the complex mechanism of breathing in a living organism with the advantage of a constant setup for all experiments. Breathing pattern, depth of inhalation and volume as well as the arterial pressure can be manipulated. Another great advantage of the IPVML is the complete control of the perfusion solution. Temperature, pH and flow rate can be adjusted according to the experimental setup. As the remaining blood is flushed out of the system, the risk of blood clots and unintended edema formation is reduced drastically. Moreover, acute effects of drugs or toxicants can be measured in the lung without the first pass effect of the liver and degradation by enzymes in the blood. Unlike in living animals, hyperventilation and stress reactions after *in vivo* application of drugs or animal handling are not observed in this system**.**

The sensitive but robust setup also produces no stress and pain due to multiple drug applications, and is therefore an important refinement according to the 3R ethical guidelines of animal experimentation. Moreover, its use in analyzing pulmonary functions of TRP channels has already been demonstrated [77, 78].

2.5 Goals of this Thesis

Ion channels and, in particular, TRP channels play a central role in many different processes in the lung. The impact of different TRP channels (TRPV4 and TRPC4) in pulmonary disease and lung toxicology needs to be elucidated. Furthermore, the IPVML model as a suitable system for detecting acute lung toxicology of drugs should be evaluated in the present thesis.

The following questions ought to be answered:

(1) Do TRPV4-deficient mice develop morphological changes in lung structure with age and how are they quantified?

(2) Does activation of TRPC4 channels by the potential cytostatic drug candidate (-) Englerin A induce changes in the lung endothelium and is the IPVML the right system to detect any acute damages?

Along these lines, both questions were answered in the following two publications with myself as co-author and first author.

3. Research paper I

JCI insight

RESEARCH ARTICLE

TRPV4 channels are essential for alveolar epithelial barrier function as protection from lung edema

Jonas Weber,[1] Suhasini Rajan,[1] Christian Schremmer,[1] Yu-Kai Chao,[1] Gabriela Krasteva-Christ,[2] Martina Kannler,[1] Ali Önder Yildirim,[3] Monika Brosien,[4] Johann Schredelseker,[1] Norbert Weissmann,[4] Christian Grimm,[1] Thomas Gudermann,[1] and Alexander Dietrich[1]

[1]Walther Straub Institute of Pharmacology and Toxicology, a member of the German Center for Lung Research (DZL), Ludwig Maximilian University of Munich, Munich Germany. [2]Institute of Anatomy and Cell Biology, School of Medicine, Saarland University, Homburg, Germany. [3]Comprehensive Pneumology Center, Institute of Lung Biology and Disease, a member of the DZL, Helmholtz Center Munich, German Research Center for Environmental Health, Munich, Germany. [4]Justus Liebig University Giessen, Cardio-Pulmonary Institute, University of Giessen and Marburg Lung Center, a member of the DZL, Giessen, Germany.

Ischemia/reperfusion-induced edema (IRE), one of the most significant causes of mortality after lung transplantation, can be mimicked ex vivo in isolated perfused mouse lungs (IPL). Transient receptor potential vanilloid 4 (TRPV4) is a nonselective cation channel studied in endothelium; however, its role in the lung epithelium remains elusive. Here, we show enhanced IRE in TRPV4-deficient ($TRPV4^{-/-}$) IPL compared with that of WT controls, indicating a protective role of TRPV4 in maintenance of the alveolar epithelial barrier. By immunohistochemistry, mRNA profiling, and electrophysiological characterization, we detected TRPV4 in bronchial epithelium, alveolar epithelial type I (ATI), and alveolar epithelial type II (ATII) cells. Genetic ablation of TRPV4 resulted in reduced expression of the water-conducting aquaporin-5 (AQP-5) channel in ATI cells. Migration of $TRPV4^{-/-}$ ATI cells was reduced, and cell barrier function was impaired. Analysis of isolated primary $TRPV4^{-/-}$ ATII cells revealed a reduced expression of surfactant protein C, and the TRPV4 activator GSK1016790A induced increases in current densities only in WT ATII cells. Moreover, $TRPV4^{-/-}$ lungs of adult mice developed significantly larger mean chord lengths and altered lung function compared with WT lungs. Therefore, our data illustrate essential functions of TRPV4 channels in alveolar epithelial cells and in protection from edema formation.

Authorship note: SR and CS contributed equally to this work.

Conflict of interest: The authors have declared that no conflict of interest exists.

Submitted: October 22, 2019
Accepted: September 9, 2020
Published: September 15, 2020.

Reference information: *JCI Insight*. 2020;5(20):e134464. https://doi.org/10.1172/jci.insight.134464.

Introduction

The alveolar epithelium has multiple functions in the lung. On the one hand, the epithelial layer forms a natural barrier to the external environment, protecting the body from invading microorganisms and toxicants, while, on the other hand, alveolar epithelial cells facilitate gas exchange. In the adult lung, the alveolar epithelium consists of 2 epithelial cell types that are crucial to maintain lung homeostasis and tissue repair (1). Alveolar epithelial type I (ATI) cells are elongated with a large surface area and high barrier function, which facilitates gas exchange in close proximity to endothelial cells of the alveolar capillaries (1). ATI cells are also highly water permeable, allowing for ion transport and maintenance of lung fluid balance (2). Although the latter cells cover the largest surface area of the lung (3), alveolar epithelial type II (ATII) cells, which exhibit a cubic morphology, by far outnumber ATI cells (4). ATII cells are also involved in ion transport and liquid homeostasis (5) and are — most importantly — responsible for the production, storage, secretion, and recycling of pulmonary surfactant. Surfactant lowers the surface tension at the tissue-air barrier to allow proper inflation and deflation of the alveoli during breathing (6). Moreover, ATII cells also serve as progenitors for ATI cells and are capable of long-term self-renewal (7). Although alveolar epithelial cells express a wide variety of ion transporters and channels (8), the exact roles of these proteins for specialized alveolar cell functions have remained elusive.

Transient receptor potential vanilloid 4 (TRPV4) is the fourth cloned member of the vanilloid family of TRP channels (9). Like most TRP channels, TRPV4 harbors an invariant sequence, the TRP box (containing the amino acid sequence EWKFAR), in its intracellular C-terminal tail as well as ankyrin repeats

JCI insight RESEARCH ARTICLE

in the intracellular N-terminus. The protein is composed of 6 membrane-spanning helices (S1–S6) and a presumed pore-forming loop between S5 and S6 (9, 10). Four of these monomers of the same type preferentially assemble in a functional homotetrameric complex (11), although TRPV4/TRPP2 complexes were also identified in cilia of renal epithelial cells (12). Homotetrameric TRPV4 was originally characterized as a sensor of extracellular osmolarity (13, 14). The channel is functionally expressed in endothelial (15, 16) and epithelial cells of the respiratory system (17–19). TRPV4 channels are thermosensitive in the range of 24°C–38°C and may additionally serve as mechanosensors, because they are activated by membrane and shear stretch as well as by viscous loading (20). As TRPV4 is also involved in pulmonary hypertension (21, 22) and bladder function (23), the channel is an interesting pharmacological target, with numerous modulators already identified (reviewed in ref. 24). Moreover, TRPV4$^{-/-}$ mice were protected from bleomycin-induced pulmonary fibrosis, due to the channel's constitutive expression and function in lung fibroblasts (25). In lung endothelium, where its role was most extensively studied, direct or indirect activation of TRPV4 by mechanical stress (26), high peak inspiratory pressure (27, 28), and high pulmonary venous pressure due to heart failure (29) resulted in the disruption of the endothelial barrier and edema formation. In other tissues, however, the channel maintains physiological cell barrier, for example, in skin (30), the urogenital tract (31), and the corneal epithelium (32). In tracheal epithelial cells, TRPV4 channels regulate ciliary beat frequency (17), and in alveolar epithelial cells, TRPV4 activation by 4α-phorbol esters produced blebs and breaks in lung septa (33) by unknown molecular mechanisms. Moreover, stimulation of TRPV4 by bacterial LPS mounted a protective response (34), whereas TRPV4 inhibition reduced lung edema and inflammation after chlorine exposure (35). Therefore, TRPV4 channels may function as chemosensors of toxicants in the lung epithelium (reviewed in ref. 36), but their exact role in the alveolar epithelium is still elusive.

We have shown that TRPC6, a member of the classical TRP channel family in the endothelium, increases endothelial permeability during ischemia/reperfusion-induced (I/R-induced) edema formation (37), one of the most significant causes of mortality after lung transplantation. However, as outlined above, endothelial permeability is also increased by TRPV4 activation (summarized in ref. 38). Along these lines, we analyzed I/R-induced edema formation in a TRPV4-deficient (TRPV4$^{-/-}$) mouse model. Surprisingly, edema development was increased in TRPV4$^{-/-}$ lungs, but edema development in TRPC6/TRPV4 double-deficient lungs was similar to that of WT lungs. These data indicate a protective role for TRPV4 channels in the other natural cell barrier of the lung, the epithelium. Therefore, we set out to study functions of TRPV4 channels in the alveolar epithelium, capitalizing on the TRPV4$^{-/-}$ mouse model. Enhanced lung edema formation triggered by I/R probably may be due to downregulation of aquaporin-5 (AQP-5) channels in ATI cells, reduced surfactant protein-C (SP-C) production in ATII cells, and/or emphysema-like changes in the overall lung architecture. Our data suggest an essential role of TRPV4 channels in the alveolar epithelium.

Results

Ablation of TRPV4 increases IR-induced edema formation in isolated perfused mouse lungs. To investigate the role of TRPV4 in IR-induced edema formation, we isolated lungs from WT and TRPV4$^{-/-}$ mice. Initial characterization of these mice revealed impaired pressure sensation in dorsal root ganglia (39) and osmotic sensation by exaggerated arginine vasopressin secretion in the brain (40). Loss of TRPV4 protein was confirmed in lung lysates. While in WT controls a protein of appropriately 100 kDa in size was detected by Western blotting with TRPV4-specific antibodies, TRPV4$^{-/-}$ lungs did not express any TRPV4 protein (Figure 1A). Murine embryonic fibroblasts (41), such as pulmonary fibroblasts, express TRPV4 protein (25) and served as an additional positive control. After initial perfusion of isolated lungs for 15 minutes, ischemia was induced for 90 minutes followed by 120 minutes reperfusion. TRPV4$^{-/-}$ lungs showed enhanced lung edema formation, as evidenced by a considerable gain in lung weight, as opposed to WT lungs (Figure 1B), which increased in weight to a similar extent as already described by us previously (37). These results clearly contrast with observations on TRPC6-deficient lungs, which are protected from IR-induced edema due to reduced endothelial permeability (37). Therefore, we generated a TRPV4/TRPC6 double-deficient mouse model (TRPV4/TRPC6$^{-/-}$), which has lungs that lack the increase in IR-induced edema formation but that developed edema, similar to WT mice (Figure 1B). Moreover, lung edema formation in TRPV4$^{-/-}$ lungs was clearly visible by the naked eye (Figure 1C), and, consistently, the wet-to-dry weight ratio increase doubled in TRPV4$^{-/-}$ lungs but only slightly increased in TRPV4/TRPC6$^{-/-}$ lungs (Figure 1D). In conclusion, TRPV4 ablation induces increased IR-induced edema, which

JCI insight

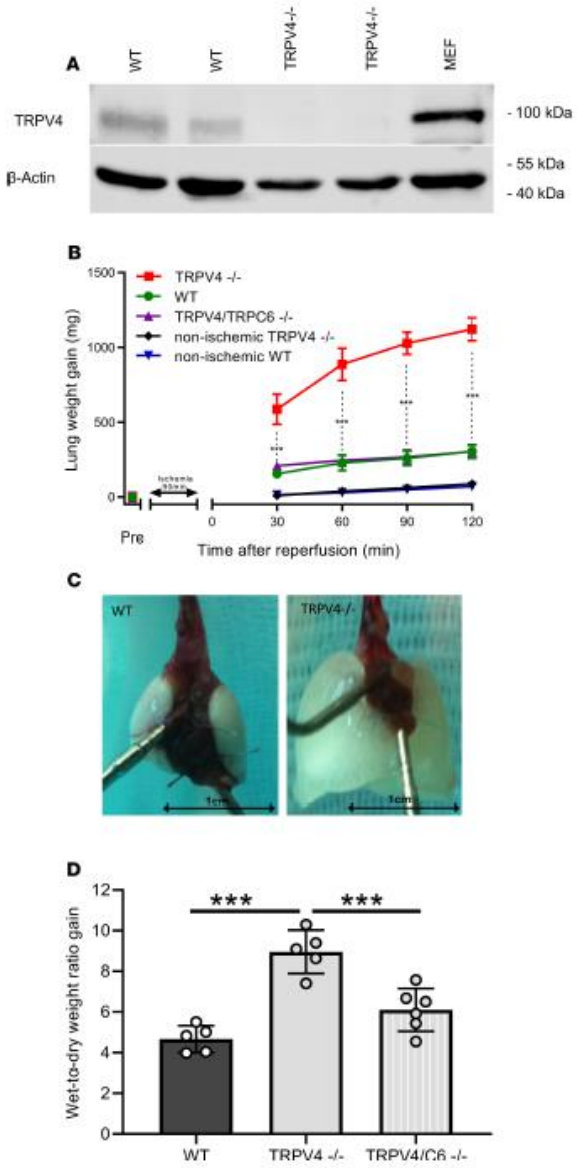

Figure 1. Ablation of TRPV4 increases ischemia-induced edema formation in mouse lungs. (**A**) TRPV4 protein expression in mouse lungs was evaluated by immunoblotting in whole-lung lysates of WT and TRPV4-deficient (TRPV4$^{-/-}$) mice using a TRPV4-specific antiserum. Murine embryonic fibroblasts (MEFs) served as an additional positive control. β-Actin was used as loading control. (**B**) Constant weight measurement of ischemic and nonischemic WT and TRPV4$^{-/-}$ and TRPV4/TRPC6 double-deficient (TRPV4/TRPC6$^{-/-}$) isolated perfused lungs. (**C**) Representative images of WT and TRPV4$^{-/-}$ lungs after ischemia. (**D**) Wet-to-dry weight ratio gains of TRPV4$^{-/-}$ and TRPV4/TRPC6$^{-/-}$ lungs compared with those of WT controls. Data represent mean ± SEM of at least 5 lungs for each genotype. Significance between means was analyzed using ANOVA (**B** and **D**); ***$P < 0.001$.

can be reduced by additional ablation of TRPC6 channels. To identify a possible role for endothelial TRPV4 channels, which might be activated by shear stress due to hydrostatic pressure (42), we decreased initial flow rates (preflow) from 2 ml to 0.5 ml/min. We did not observe any major changes in edema formation in ischemic and nonischemic WT lungs. TRPV4$^{-/-}$ lungs showed a significantly decreased edema

formation only after 90 and 120 minutes of reperfusion for unknown reasons (see Supplemental Figure 1; supplemental material available online with this article; https://doi.org/10.1172/jci.insight.134464DS1).

TRPV4 is expressed in ATI and ATII cells. As TRPV4 is highly expressed in lung endothelium, and its activation results in an increase of endothelial permeability (reviewed in ref. 38), we focused on its possible functions in the epithelium. Epithelial cells represent the second natural barrier regulating edema formation. Analysis of mice carrying an EGFP reporter protein under the control of the TRPV4 promoter/enhancer region revealed expression of TRPV4 protein in endothelium as well as bronchial and alveolar epithelium (Figure 2A). In the bronchial epithelium we detected TRPV4 in ciliated cells by costaining with a β-tubulin IV antibody (Supplemental Figure 2, A–C). Neither club nor neuroendocrine cells showed TRPV4 expression (Supplemental Figure 2, D–I). In the alveoli, costaining experiments with an antibody directed against AQP-5 (Figure 2B), a marker protein of ATI cells, which are involved in lung septa formation (2), revealed a red staining indicative of AQP-5 expression in the plasma membrane and an additional green staining of the cytosol, reflecting TRPV4 expression in these cells (Figure 2B, inset). Moreover, direct quantification of TRPV4 mRNA revealed similar expression levels in ATII cells as in lung endothelial cells, but lower mRNA expression in pulmonary murine lung fibroblasts and precapillary arterial smooth muscle cells (Figure 2C). Therefore, TRPV4 channels are expressed in ATI and ATII cells of the alveolar epithelium.

Loss of TRPV4 resulted in decreased AQP-5 expression in ATI cells. Staining of lung slices with fluorescence-coupled antibodies specific for the water-conducting channel AQP-5 revealed lower total expression levels in ATI cells and reduced plasma membrane localization in TRPV4$^{-/-}$ lungs compared with that in WT lungs (Figure 3, A–E). These results were confirmed by Western blotting of lung lysates probed with an AQP-5–specific antibody (Figure 3, F and G). In clear contrast to these results, protein levels of AQP-1, a major aquaporin channel in the microvascular endothelium, were not significantly different in TRPV4$^{-/-}$ cells compared with WT endothelial cells (Supplemental Figure 3, A–E). Therefore, AQP-5 protein levels in the alveolar epithelium, but not AQP-1 expression in the endothelium is reduced by ablation of TRPV4.

Identification of currents induced by the TRPV4 activator GSK1016790A only in primary ATII cells from WT mice. To investigate the role of TRPV4 on at a cellular level, we first isolated ATII epithelial cells (Figure 4A) from WT and TRPV4$^{-/-}$ mice. We were not able to detect any morphological differences in ATII cells of the different genotypes by phase-contrast microscopy. ATII cells were identified by staining with fluorophore-coupled antibodies directed against directed against prosurfactant protein C (pSP-C) (Figure 4B), which is secreted by ATII cells (reviewed in ref. 5). Patch clamp analysis of primary ATII cells revealed significantly larger currents, which were induced by the selective TRPV4 activator GSK1016790A (GSK, reviewed in ref. 24) only in WT cells, while currents after the application of GSK in TRPV4$^{-/-}$ cells were not significantly different compared with basal currents in WT cells (Figure 4, C and D). Western blotting of protein lysates from ATII cells revealed lower pSP-C levels in TRPV4$^{-/-}$ ATII cells compared with WT cells (Figure 4, E and F). We then differentiated ATII cells to ATI cells by growing them to confluence in plastic cell culture dishes for at least 6 days as described previously (1) (Figure 4G). After 6 days, WT cells expressed AQP-5 protein as an ATI cell marker (Figure 4H). In conclusion, TRPV4 channels are functionally active in ATII cells and are involved in the expression of pSP-C of these alveolar epithelial cells, which can be differentiated to ATI cells in vitro.

TRPV4$^{-/-}$ ATI cells express less AQP-5, show reduced nuclear localization of NFAT, and decreased cell migration and adhesion. As already shown in lung sections of TRPV4$^{-/-}$ mice, translocation of AQP-5 to the plasma membrane was reduced in TRPV4$^{-/-}$ cells (Figure 5, A and B). To test if TRPV4$^{-/-}$ ATII cells are able to differentiate to ATI cells, we analyzed the expression of podoplanin (T1α), another ATI cell marker protein. Notably, podoplanin expression was not significantly different in TRPV4$^{-/-}$ ATII cells differentiated to ATI cells (Figure 5, C and D).To further analyze ATI cell function, we quantified nuclear NFATc1 levels. The translocation of NFATc1 protein to the nucleus was significantly reduced in TRPV4$^{-/-}$ cells (Figure 5, E and F). Moreover, cell migration analyzed by gap closure in in vitro experiments was clearly slowed down in TRPV4$^{-/-}$ ATI cells compared with WT cells (Figure 5, G and H). As an additional line of evidence, we transfected ATII cells with TRPV4-specific or control siRNAs, differentiated them to ATI cells, and quantified cell migration in the same way (Supplemental Figure 4). Most interestingly, we obtained similar results in cells transfected with TRPV4 siRNA, which showed a significantly slower migration compared with non-transfected cells as well as cells transfected with the control siRNAs. As determined by electrical cell impedance sensing (ECIS), subconfluent TRPV4$^{-/-}$ ATI cells showed reduced cell barrier function (Figure 5I).

JCI insight RESEARCH ARTICLE

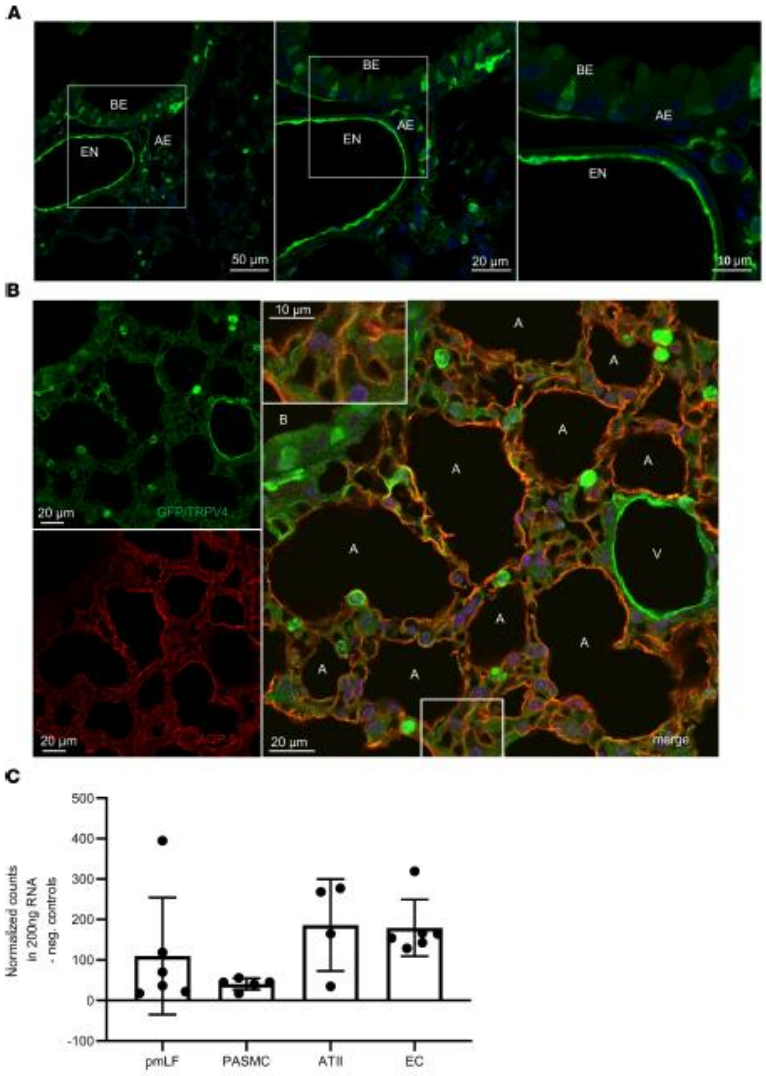

Figure 2. TRPV4 and aquaporin-5 expression in mouse lungs. (**A**) GFP staining (green) by fluorescence-coupled GFP-specific antibodies in lung cryosections of TRPV4EGFP reporter mice reveals expression of TRPV4 in cells of the lung endothelium (EN) as well as in the bronchial (BE) and alveolar epithelium (AE). Nuclei staining was performed with Hoechst dye (blue). Scale bar: 10 µm (right); 20 µm (middle); 50 µm (left). (**B**) Lung cryosections from TRPV4EGFP reporter mice were stained with fluorescence-coupled antisera directed against GFP and aquaporin-5 (AQP-5). Confocal images were obtained after excitation at 488 nm (for EGFP, left top, green) or after excitation at 561 nm (for AQP-5, left bottom, red). Both images were merged (right). Nuclei staining was performed with Hoechst dye (blue). A, alveolus; B, bronchus; V, vasculature. The inset shows the bottom boxed region in at higher magnification. Scale bar: 10 µm (inset); 20 µm. (**C**) TRPV4 mRNA quantification in lung cells using NanoString technology. ATII, alveolar type II cells; EC, endothelial cells; PASMC, precapillary arterial smooth muscle cells; pmLF, primary murine lung fibroblasts. Data represent mean ± SEM from at least 3 independent cell isolations.

Therefore, ablation of TRPV4 induced less AQP-5 expression, reduced nuclear localization of nuclear factor of activated T cells (NFAT), and reduced cell migration and cell barrier function.

TRPV4$^{-/-}$ mice showed emphysema-like lung structure and altered lung function. To analyze differences in lung anatomy as a consequence of altered ATI cell function, we quantified mean chord lengths (MCLs) in histological lung sections (Figure 6A). TRPV4 ablation significantly increased MCL of the alveolar lumen in adult (47–52 week old, Figure 6D) mice compared with WT lungs, while young mice (4–6 weeks old) showed no differences (Figure 6B). Lungs from 28- to 30-week-old mice were also prone to larger MCLs (Figure 6C), which, however, were not significantly different compared with those of WT lungs.

JCI insight RESEARCH ARTICLE

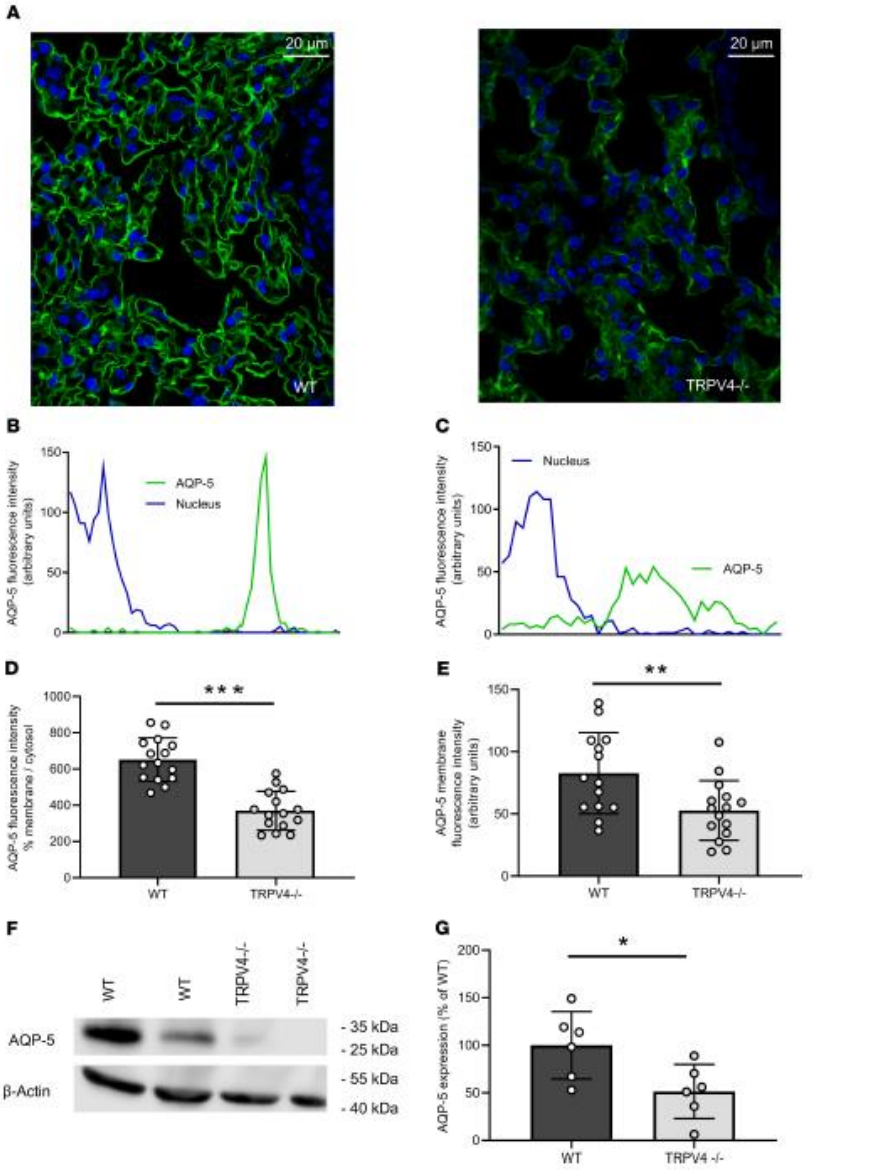

Figure 3. Aquaporin-5 expression and translocation to the plasma membrane in WT and TRPV4$^{-/-}$ alveolar epithelial type I cells. (**A**) Cryosections of WT and TRPV4$^{-/-}$ lungs stained with an aquaporin-5–specific (AQP-5–specific) fluorescence-coupled antibody. Nuclei staining was performed with Hoechst dye (blue). Scale bar: 20 µm. Representative histograms for the quantification of AQP-5 protein in the plasma membrane of WT (**B**) and TRPV4-deficient alveolar epithelial type I (ATI) cells (**C**). (**D** and **E**) Summaries of AQP-5 protein expression in plasma membranes (**D**, percentage of aquaporin-5 membrane/cytosol; **E**, percentage AQP-5 in membranes). Representative Western blot analysis of AQP-5 expression in WT and TRPV4$^{-/-}$ whole-lung lysates (**F**) and summary of AQP-5 expression in lung lysates of TRPV4$^{-/-}$ and WT mice (**G**). Data represent mean ± SEM from at least 6 lungs for each genotype. Significance between means was analyzed using 2-tailed unpaired Student's *t* test; $^{*}P < 0.05$, $^{**}P < 0.01$, $^{***}P < 0.001$.

JCI insight RESEARCH ARTICLE

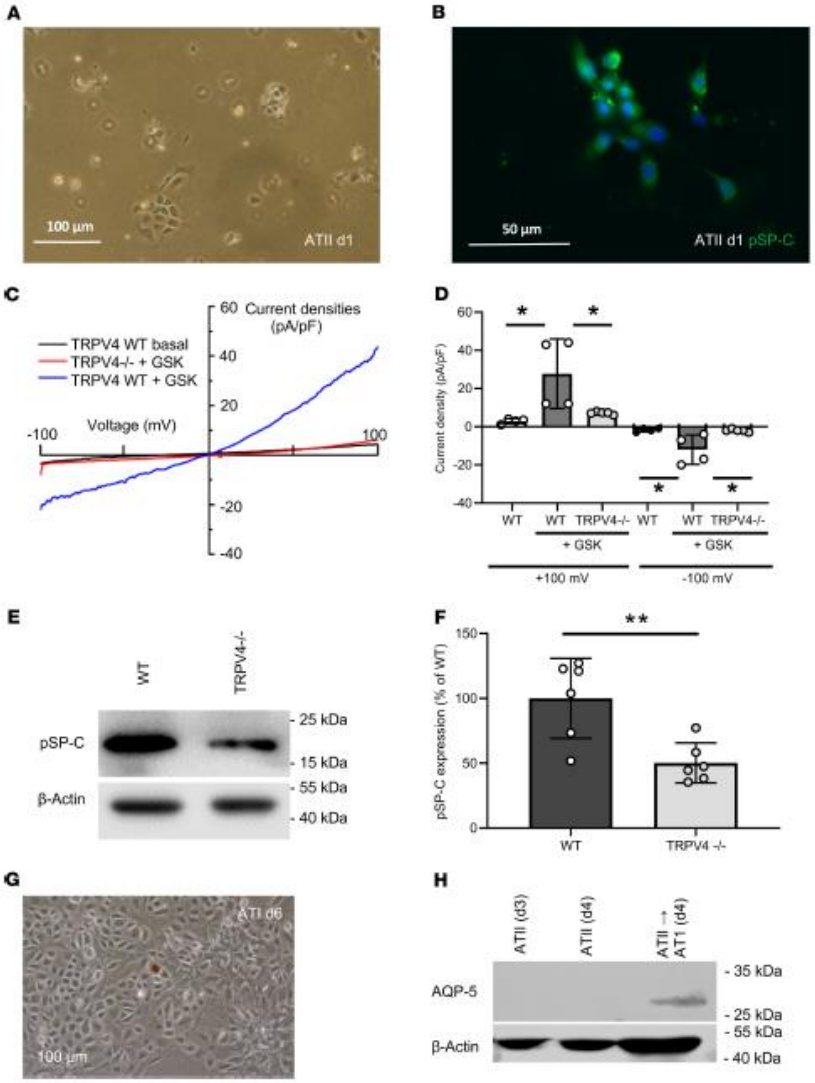

Figure 4. Identification of alveolar epithelial type II cells and differentiation to alveolar epithelial type I cells. Representative cell cluster 1 day after isolation in a phase-contrast image (scale bar: 100 µm) (**A**) and stained with a fluorescence-coupled specific pro-surfactant protein-C (pSP-C) antibody (scale bar: 50 µm) (**B**). Nuclei staining was performed with Hoechst dye (blue). Electrophysiological whole-cell measurements of basal and GSK-induced (GSK-induced) current densities in WT and TRPV4$^{-/-}$ primary alveolar epithelial type II (ATII) cells (**C** and **D**). Representative current density–voltage curves of WT (gray, blue traces) and TRPV4$^{-/-}$ (red trace) ATII cells before (gray trace) and during application of GSK (blue and red traces) (**C**). Summary of current densities at ±100 mV before (white bars) and after application of GSK analyzed in WT (black bars) and TRPV4$^{-/-}$ (gray bars) ATII cells (**D**). Representative Western blot analysis of pSP-C expression in WT and TRPV4$^{-/-}$ ATII cells (**E**) and summary of pSP-C expression in TRPV4$^{-/-}$ and WT ATII cells (**F**). Image of confluent cells on day 6 after ATII cell isolation (scale bar: 100 µm) (**G**) and analysis of AQP-5 expression in cells grown for 3, 4, and 6 days in plastic cell culture dishes by Western blotting (**H**). β-Actin was used as loading control in each blot. Data represent mean ± SEM from at least 3 independent cell preparations of 5 mice each. Significance between means was analyzed using 1-way ANOVA (**C**) or 2-tailed unpaired Student's *t* test (**F**); $^{*}P < 0.05$, $^{**}P < 0.01$.

JCI insight RESEARCH ARTICLE

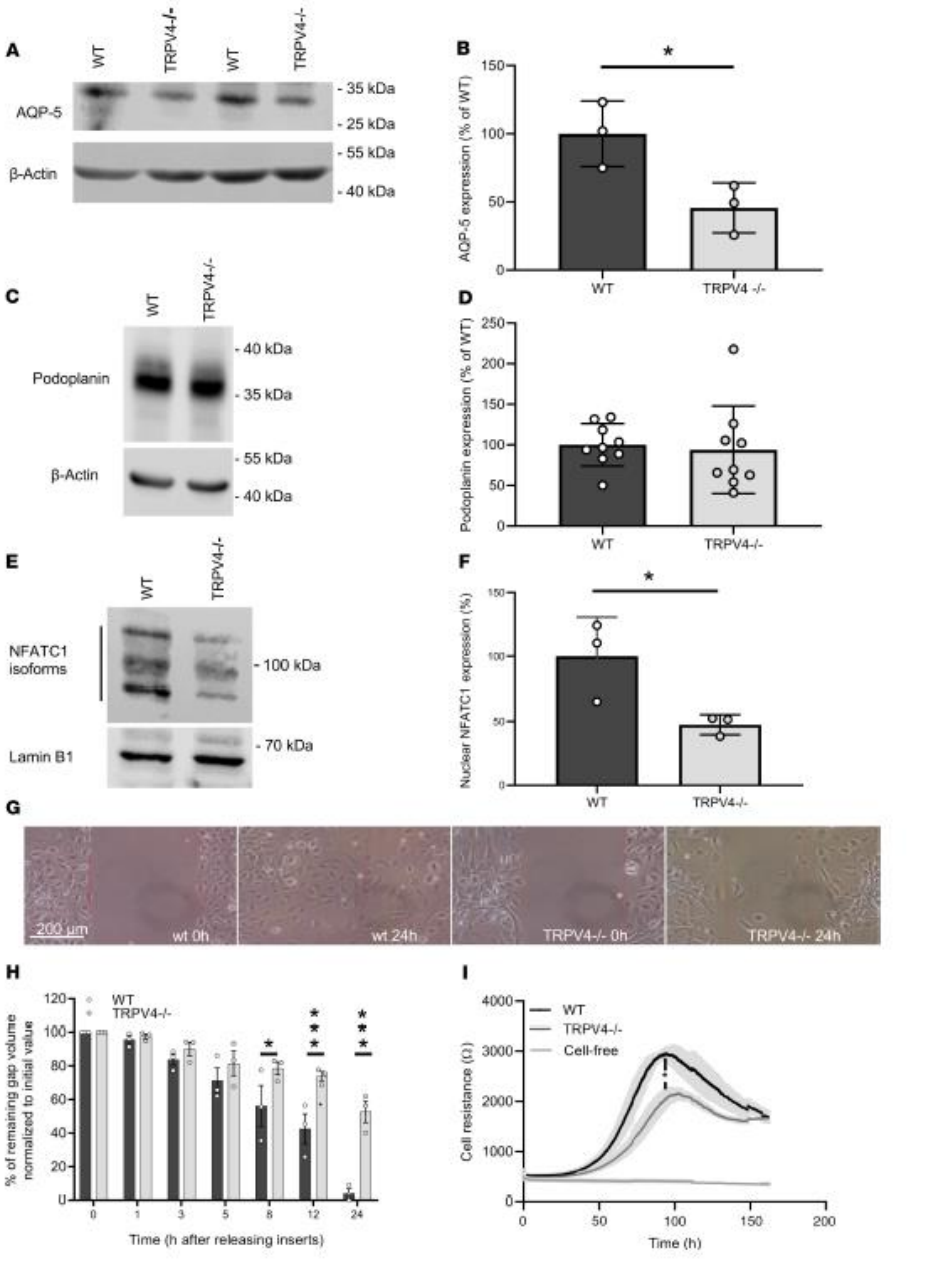

JCI insight RESEARCH ARTICLE

Figure 5. Nuclear localization of nuclear factor of activated T cells in and migration and adhesion of TRPV4-deficient and WT ATI cells. Representative Western blot analysis of AQP-5 expression in WT and TRPV4$^{-/-}$ ATII cells differentiated to ATI cells (**A**) and summary of AQP-5 expression in these cells (**B**). Representative Western blot analysis of podoplanin expression – another ATI cell marker – in WT and TRPV4$^{-/-}$ ATII cells differentiated to ATI cells (**C**) and summary of podoplanin expression in these cells (**D**). Representative Western blot analysis of nuclear NFATc1 localization in WT and TRPV4$^{-/-}$ ATI cells (**E**) and summary of nuclear factor of activated T cells (NFAT) localization in these cells (**F**). Lamin B1 served as loading control. Representative images of a migration assay after removing inserts (scale bar: 200 μm) (**G**). Summary of remaining gap values normalized to initial values quantified in migration assays of TRPV4$^{-/-}$ and WT ATI cells after releasing inserts at 0, 1, 3, 5, 8, 12, and 24 hours (**H**). Electrical cell resistance was quantified with an ECIS device for WT and TRPV4$^{-/-}$ ATI cells for 160 hours. (**I**). Data represent mean ± SEM from at least 3 independent cell preparations of 5 mice each. Significance between means was analyzed using 2-tailed unpaired Student's *t* test; $^{*}P < 0.05$, $^{***}P < 0.001$.

Moreover, lung function was altered (Figure 6, E–H): TRPV4$^{-/-}$ lungs showed increased inspiratory capacity and compliance (Figure 6, E, G, and H) as well as decreased elastance (Figure 6F), which was significantly different from that of WT mice of the same age. In conclusion, adult TRPV4$^{-/-}$ mice showed emphysema-like changes in their lungs, which may be responsible for altered lung function.

Discussion

Although TRPV4 is highly expressed in lungs, its exact function is still elusive (reviewed in ref. 24). Activation of TRPV4 in endothelial cells by mechanical stress, for example, stretching (27, 28, 43), as well as oxidative stress by exposure to H_2O_2 (44) resulted in an increased Ca^{2+} influx mediated by the channel and an increase in endothelial permeability conducive to lung edema (reviewed in ref. 38). Along these lines, pharmacological blockade of TRPV4, for example, by the specific blocker HC-067047, decreased intracellular Ca^{2+} levels in endothelial cells and protected mice from vascular leakage and lung injury (28). Expression and function of TRPV4 channels in the alveolar epithelium, however, has not been studied yet.

Here, we quantified IR-induced edema as one of the most common and significant causes of morbidity and mortality after lung transplantation (45), using the isolated perfused lung model (37). Much to our surprise, TRPV4$^{-/-}$ lungs were not protected from IR-induced lung edema, as observed in TRPC6$^{-/-}$ mice (37). On the contrary, genetic TRPV4 ablation resulted in a robust increase in lung edema (Figure 1B) and a higher wet-to-dry weight ratio increase (Figure 1D) when compared with that of control WT mice. Barrier function was rescued by consecutive breeding of TRPV4$^{-/-}$ mice with TRPC6$^{-/-}$ mice, because lung edema formation in double-deficient mice was similar to that in WT animals (Figure 1B).

As TRPV4 activation in endothelial cells has been shown to result in higher edema formation, we focused on the lung epithelium, another physiological cell barrier in the lung. Recent publications indicate an epithelial function of the channel opposed to that in endothelium, i.e., stabilization of the epithelial barrier in the skin (30), the urogenital tract (31), and the corneal epithelium (32). We demonstrated TRPV4 expression in ATI and ATII cells (Figure 2, B and C). Our further molecular analysis corroborated a functional link between TRPV4 and AQP-5, a water-conducting channel expressed in ATI cells (46). Hypotonic solutions increased the association and surface localization of TRPV4 and AQP-5 in salivary gland cells (47), and AQP-5 expression is regulated by TRPV4 in lung epithelial cells (48). Most interestingly, the expression and plasma membrane translocation of AQP-5 channels in ATI cells were significantly reduced (Figure 3). Therefore, TRPV4 channels increase AQP-5 expression and translocation in ATI cells in clear contrast to human bronchial epithelial cells, where it has been reported that activation of TRPV4 channels by shear stress decreased AQP-5 levels (47). To analyze TRPV4 function on a cellular level, we isolated ATII cells identified by their expression of pSP-C (Figure 4, A and B). We detected significantly larger currents induced by the TRPV4 activator GSK in WT but not in TRPV4$^{-/-}$ ATII cells (Figure 4, C and D). To our knowledge, these data show for the first time that TRPV4 channels are not only expressed, also functional in ATII cells. Quantifying pSP-C levels by Western blotting revealed a reduced expression in TRPV4$^{-/-}$ cells compared with that in WT cells (Figure 4, E and F). The role of surfactant proteins in the prevention of alveolar edema by reducing surface tension as a driving force for fluid flow across the air-blood barrier is still a matter of debate (49) but might also explain exaggerated edema formation in TRPV4$^{-/-}$ mice. Therefore, functional TRPV4 and TRPC6 channels are not only located in different cell types, such as alveolar epithelial and lung endothelial cells, respectively, but may have different roles by decreasing or increasing IR-induced edema. TRPV4 channels aid in epithelial barrier function by supporting SPC production and reducing edema formation in a chronic manner, while TRPC6 channels acutely increase endothelial permeability during IR-induced edema formation (37). Although we cannot exclude a role for endothelial TRPV4 channels, it is unlikely that TRPV4 channels in the endothelium are activated

JCI insight RESEARCH ARTICLE

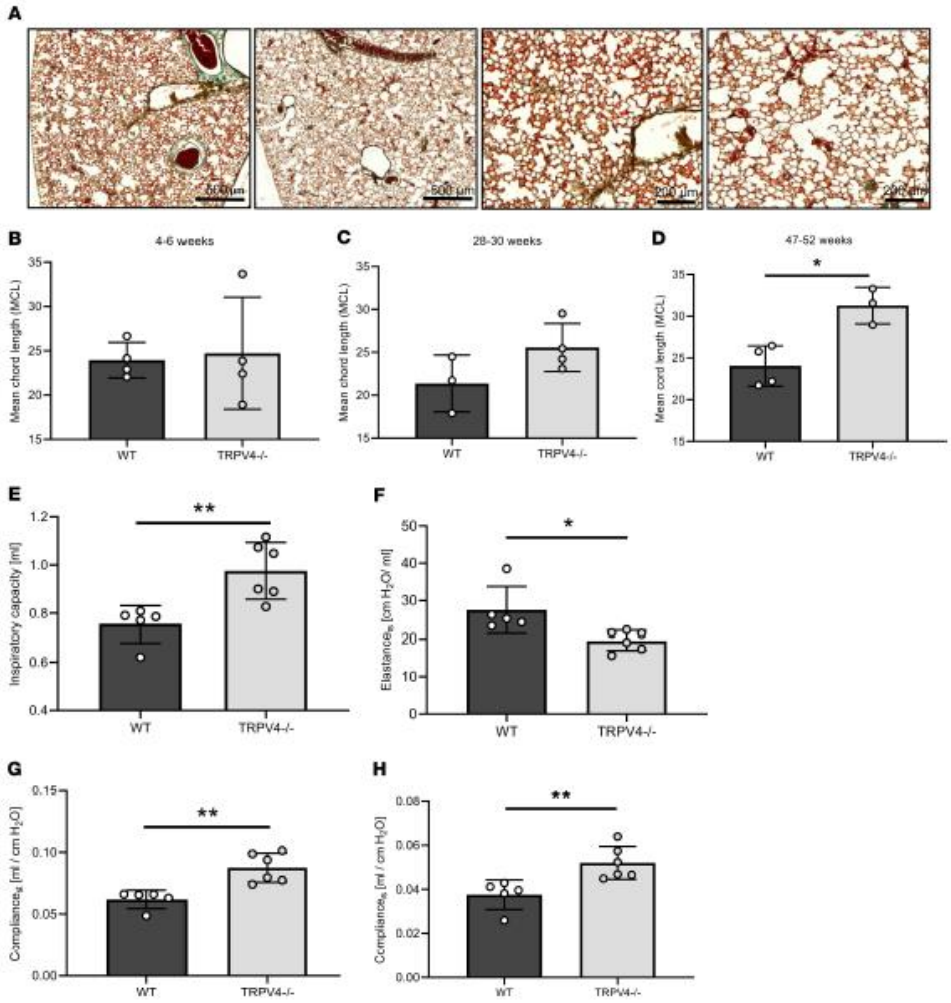

Figure 6. Chord lengths and lung function of WT and TRPV4$^{-/-}$ mice. Representative images of Masson's trichrome–stained lung sections from 52-week-old WT (left, scale bar: 500 µm) and TRPV4$^{-/-}$ mice (right, scale bar: 200 µm) (**A**). Quantification of mean chord lengths of 4- to 6- (**B**), 28- to 30- (**C**), and 47- to 52-week-old (**D**) WT and TRPV4$^{-/-}$ mice. Inspiratory capacity (**E**), elastance of the respiratory system (**F**), static compliance (C_{rs}, **G**) and compliance of the respiratory system (C_{rs}, **H**) of 6-month-old WT and TRPV4$^{-/-}$ mice. Data represent mean ± SEM from at least 3 mice. Significance between means was analyzed using 2-tailed unpaired Student's *t* test; $^*P < 0.05$, $^{**}P < 0.01$.

by shear stress due to hydrostatic pressure, as reducing the preflow in the experiments had no effect on IR-induced edema formation (Supplemental Figure 1).

Next, we differentiated ATII cells to ATI cells (1), monitored by the expression of 2 ATI cell markers: AQP-5 and podoplanin. As AQP-5 protein expression was reduced in TRPV4$^{-/-}$ ATI cells (Figure 5, A and B), while podoplanin levels were not altered (Figure 5, C and D), it seems rather unlikely that TRPV4

deficiency and/or a reduction of pSP-C expression results in reduced ATII cell to ATI cell differentiation in general. Plasma membrane translocation of AQP-5 as well as AQP-5 expression may depend on nuclear localization of the transcription factor NFAT by an increase of intracellular Ca^{2+} via TRPV4 similar to TRPC channels (50). Therefore, we quantified nuclear NFAT levels and detected significantly lower levels in TRPV4$^{-/-}$ cells in comparison with that in WT control cells (Figure 5, E and F). A major breakthrough in our understanding of AQP-5 function for water transport across apical membranes of ATI cells was the analysis of AQP-5–deficient mice (51). Although lack of AQP-5 entailed a 10-fold decrease in alveolar permeability in response to an osmotic gradient, AQP-5$^{-/-}$ mice are indistinguishable from WT mice with regard to hydrostatic pulmonary edema as well as isoosmolar fluid transport from the alveolar space (51, 52). Cognizant of this scenario, a role for AQP-5 in the clearance of fluid from the alveolar space after IR-induced lung edema cannot entirely be ruled out, but it appears to be unlikely, and we tried to dissect other additional mechanisms for the vulnerability of TRPV4$^{-/-}$ lungs to edema formation.

As 2 reports demonstrated decreased migration of human epithelial ovarian cancer (53) or endometrial adenocarcinoma cells (54) after downregulation of AQP-5, we set out to quantify cell migration of ATII cells differentiated to ATI cells. TRPV4$^{-/-}$ ATI cells showed a clear deficit in closing gaps by cell migration after releasing inserts compared with WT cells (Figure 5, G and H). In additional experiments, we were able to reproduce these results in cells transfected with TRPV4 siRNAs compared with nontransfected cells as well as cells transfected with control siRNAs (Supplemental Figure 4). These data suggest an important role of TRPV4 channels in cell migration, which needs to be further analyzed in the future. Moreover, cell resistance, as analyzed by ECIS, was significantly reduced in growing TRPV4$^{-/-}$ ATI cells in contrast to that in WT cells (Figure 5I). Both cell types, however, reached confluence after 160 hours, excluding gross changes in their proliferation rates. Changes in cell morphology were also not detected by microscopy.

ATII cells are able to differentiate to ATI cells after lung injury during repair processes in adult mice (7) to reestablish barrier function of the lung alveolus. Therefore, we analyzed lung alveolar histology in WT and TRPV4$^{-/-}$ lungs in young and adult mice. MCL as a measure of alveolar size was increased in adult (47–52 weeks old) but not in young (3 weeks old) TRPV4$^{-/-}$ mice compared with WT mice of the same ages (Figure 6, A–D). We concluded that differences were not caused by defects in embryonic lung development but were due to ongoing growth and repair processes in adult animals. Most interestingly, the emphysema-like changes in lung morphology were also detected in SP-C–deficient mice (55), raising the possibility that reduced SP-C levels in TRPV4$^{-/-}$ ATII cells may also contribute to the phenotype. In the same vein, adult TRPV4$^{-/-}$ mice showed altered lung function, with increased inspiratory capacity and compliance as well as decreased elastance (Figure 6, E–H) compared with WT mice of the same ages. Loss of septa formation because of reduced SP-C levels in adult TRPV4$^{-/-}$ mice may be responsible for decreased clearance of fluid from the alveolar space and may therefore explain higher levels of edema formation in TRPV4$^{-/-}$ lungs.

In summary, loss of TRPV4 channels in alveolar epithelial cells results in decreased pSP-C production in ATII cells and lower AQP-5 expression and membrane localization in ATI cells. The latter proteins are likely to be involved in continuously ongoing repair processes in adult mice, resulting in emphysema-like changes in TRPV4$^{-/-}$ mice. These chronic events may define a protective function of TRPV4 channels against lung edema formation, in clear contrast to their acute detrimental role in endothelial cells.

Methods

Animals. TRPC6$^{-/-}$ (56) and TRPV4$^{-/-}$ (B6.199X1-Trpv4^{tm1MSZ} from Riken BioResource Center, RBRC01939) (39, 40) mice were backcrossed 10 times to the C57/BL6J strain. TRPC6/TRPV4$^{-/-}$ mice were obtained by crossing both gene-deficient mouse models. TRPV4EGFP reporter mice (Tg(TRPV4-EGFP)MT43Gsat/Mmucd from MMRC) were bred as previously described (57). Sex- and age-matched mice older than 3 months were used in the experiments, if not mentioned otherwise in the figure legends.

Isolated, perfused mouse lung. Quantification of edema formation in isolated perfused mouse lungs was done as described previously (37). In brief, mice were anesthetized by intraperitoneal injection of ketamine (100 mg/kg BW), xylazine (0.7 mg/kg BW), and anticoagulated with heparin (500 IU/kg BW). Animals were intubated via a small incision in the trachea, ligated, and ventilated with room air using the VCM type 681 (positive end–expiratory pressure, 3 cmH_2O; positive end–inspiratory pressure 3 cmH_2O; respiratory rate was 90 breaths/min). The sternum was opened, the ribs were spread, and the right ventricle was incised

to place the air-free perfusion catheter into the pulmonary artery. After ligation, the perfusion was started with 0.5 ml/min perfusion solution (7.19 g sodium chloride, 0.33 g potassium chloride, 0.27 g magnesium hexahydrate, 0.36 g calcium chloride dihydrate, 0.15 g potassium dihydrogen orthophosphate, 2.67 g glucose monohydrate, 51.28 g hydroxyethyl starch [type 2000000/05] ad 1000 mL with aqua ad iniectabilia, and 0.1848 mg/mL sodium hydrogen carbonate to adjust pH to 7.3) using an ISMATEC Tubing Pump. A second perfusion catheter was introduced in the left ventricle and secured by ligation. The lung, the trachea, and the heart were excised from the thorax in 1 piece and transferred to a 37°C temperature-equilibrated housing chamber for the perfused mouse lung model (IPL-2, Hugo Sachs Elektronik/Harvard Apparatus). The perfusion was slowly raised stepwise to 2 ml/min, and perfusion pressure was monitored with the PLUGSYS TAM-A/P75 type 17111 (Harvard Apparatus). Weight changes were constantly measured with the edema Balance Module/EBM type 713 (Harvard Apparatus). Data were monitored with Pulmodyn software (Harvard Apparatus). The perfusion pressure during the measurements was not significantly different between genotypes as well as before and after ischemia.

Analysis of functional parameters of the respiratory tract. Mice were anesthetized with ketamine (270 mg/kg BW) and xylazin (11 mg/kg BW), intratracheally intubated through a small incision of the trachea, and connected to the flexiVent system (Scireq).

Immunohistochemistry. Mouse lungs were inflated with 2.5% (m/v) glutaraldehyde in PBS and processed for paraffin or O.C.T. compound (Tissue-Tek, Sakura Finetek) embedding. Paraffin-embedded tissue sections (3 μm) were cut using a microtome (Zeiss), mounted on glass slides, deparaffinized in xylene, and rehydrated in graded alcohol. Masson Goldner trichrome staining (Masson Goldner Trichrome Staining Kit, Carl Roth 3459) was done according to the manufacturer's instruction with iron hematoxylin solution for 8 minutes, Goldner's stain 1 for 6 minutes, Goldner's stain 2 for 1 minute, and Goldner's stain 3 for 5 minutes. After dehydration in 100% EtOH and clearing in xylol twice for 1 minute, the sections were mounted in Roti-Histokit II (Carl Roth T160.2). Sections were analyzed by design-based stereology using an Olympus BX51 light microscope equipped with the new Computer Assisted Stereological Toolbox (newCAST, Visiopharm) as described previously (58). For MCL measurements, 10–20 frames were selected randomly across multiple sections by the software, using the ×20 objective, and superimposed by a line grid and points. The intercepts of lines on alveolar wall (Lsepta) and points localized on air space (Pair) were counted and calculated as follows: MCL ($\sum$Pair × L(p)/$\sum$Isepta × 0.5, where L(p) is the line length per point). Cryo-embedded lungs were cut in 10 μm sections on a cryostat (Leica), mounted on glass slides, and surrounded with a hydrophobic pen (Vector Laboratories). After washing with PBS, the sections were blocked for 30 minutes in PBS containing 0.2% Triton X-100 and 5% NGS. Incubation with primary antibody was done at 4°C overnight and secondary antibody at room temperature for 1 hour. Antibodies were diluted in blocking solution. After nuclei staining with Hoechst dye (Thermo Fisher Scientific) (2 μg/mL) for 5 minutes at room temperature followed by sufficient washing the sections were mounted in Roti-Histokit II. The following antibodies and dilutions were used: anti-GFP (chicken, Thermo Fisher Scientific, A10262, 1:200), anti–β-tubulin IV (rabbit monoclonal, Abcam, 179509, 1:1600), anti–AQP-1 (rabbit, Alomone Labs, AQP-001, 1:100), anti–AQP-5 (rabbit, Alomone Labs, AQP-005, 1:100), anti-CC10 (mouse, Santa Cruz Biotechnology, E-11, 1:200), anti-chicken (goat, Thermo Fisher Scientific, A11039, 1:400), anti-CGRP (goat, 1:400, Acris, BP022), anti-rabbit IgG (goat, coupled to Alexa Fluor 488, Thermo Fisher Scientific, A32731, 1:500 and donkey, coupled to Cy3, Merck Millipore, AP182C, 1:1000), and anti-goat IgG (donkey, Life Technologies, A11058, 1:400). For direct labeling of the anti-CC10 antibody, the Zenon Alexa Fluor 546 mouse IgG$_1$ kit was used according to the manufacturer's recommendations (Invitrogen, 25004). Stained cryosections were analyzed on an epifluorescence microscope (Zeiss Imager.M2, Carl Zeiss) and on a confocal microscope (LSM 880, Carl Zeiss). For membrane localization analysis, staining intensity was analyzed along a line from the nucleus into the cytosol and the plasma membrane.

Primary murine alveolar epithelial cells. Isolation of ATII cells was done as described previously (1, 59, 60). In brief, lungs were flushed via a catheter through the pulmonary artery with 0.9% NaCl solution (B. Braun Melsungen AG), inflated with 1 mL dispase (BD Biosciences), followed by 500 μl 1% low-melting-point agarose (MilliporeSigma), and incubated for 1 hour at room temperature. Subsequently, lung lobes were separated and dissected using 2 forceps; filtered through 100 μm, 20 μm, and 10 μm nylon filters (Sefar); and centrifuged for 10 minutes at 200*g*. Cell pellets were resuspended in DMEM (MilliporeSigma) and plated on CD45- and CD16/32-coated (BD Biosciences) culture dishes

JCI insight RESEARCH ARTICLE

Table 1. List of siRNAs used for downregulation of TRPV4 mRNA

Name	Target sequence
Accell mouse TRPV4 siRNA- SMARTpool	
Accell SMARTpool siRNA A-040742-13	CCAUUGACCUGUUGGAGUC
Accell SMARTpool siRNA A-040742-14	GCAACAUGCGUGAAUUCAU
Accell SMARTpool siRNA A-040742-15	UUACCAGUAUCAAAGACUU
Accell SMARTpool siRNA A-040742-16	CUCUUGUGUAUUAUUUAUU
Accell Nontargeting Pool	
Accell Nontargeting Pool D-001910-10-20	UGGUUUACAUGUCGACUAA
	UGGUUUACAUGUUUUCUGA
	UGGUUUACAUGUUUUCCUA
	UGGUUUACAUGUUGUGUGA

for a negative selection of macrophages and lymphocytes and incubated for 30 minutes at 37°C. Non-adherent cells were collected and seeded on uncoated dishes to negatively select fibroblasts at 37°C for 25 minutes. Cells were collected and identified by staining with a fluorescent coupled anti pSP-C antibody (Chemicon International, AB3786, 1:20000). Live cells were counted by trypan blue staining in a Neubauer counting chamber. 2×10^6 cells/well of a 6-well plate were seeded in DMEM containing 10% FCS (Invitrogen), 1% HEPES (Carl Roth), and 1% penicillin/streptomycin (Lonza), and used for analysis or grown for at least 6 days for ATI cell differentiation. ATII cells were transfected with 1 μM Accell SMARTpool siRNA for TRPV4 (in starving medium, 0.1% FCS) 2 days after isolation. On day 6, the cells were washed once and kept in starving medium. A noncoding pool of the Accell siRNA in starving medium served as control (see Table 1 for siRNA sequences).

Patch-clamp recordings of ATII cells. Conventional whole-cell recordings were carried out at room temperature 24 hours after isolation of ATII cells from WT and TRPV4$^{-/-}$ mice. The following bath solution, containing 140 mM NaCl, 1.3 mM $MgCl_2$, 2.4 mM $CaCl_2$, 10 mM glucose, 10 mM HEPES (pH 7.4 with NaOH) and resulting in an osmolality of 310 mOsm/kg, was used for patch-clamp recordings. The pipette solution contained 135 mM CsCl, 2 mM Na-ATP, 1 mM $MgCl_2$, 5 mM EGTA, and 10 mM HEPES (pH 7.2 with CsOH), resulting in an osmolality of 296 mOsm/kg. Patch pipettes made of borosilicate glass (Science Products) had resistances of 2.2–3.5 MΩ for whole-cell measurements. Data were collected with an EPC10 patch clamp amplifier (HEKA) using the Patchmaster software. Current density-voltage relations were obtained before and after application of the TRPV4 activator GSK (1 mM) to the bath solution using voltage ramps from –100 to +100 mV, each lasting 5 seconds. Data were acquired at a frequency of 40 kHz after filtering at 2.8 kHz. The current density-voltage curves and the current density amplitudes at ±100 mV were extracted at minimal or maximal currents, respectively.

Western blot analysis. Western blotting was done as previously described (61). Chemiluminescence was detected in an Odyssey Fc unit (Licor). The following antibodies and dilutions were used: HRP-conjugated anti–β-actin antibody (MilliporeSigma, A3854HRP, 1:10000), anti-TRPV4 (rabbit, Abcam, ab 39260, 1:1000), anti–AQP-5 (rabbit, Alomone AQP-005, 1:1000), anti-Podoplanin (goat, R&D Systems, AF3244, 1:500), secondary anti-goat IgG (whole molecule) peroxidase (MilliporeSigma, A5420-1ML, 1:10000), and secondary anti-rabbit IgG peroxidase (POX) antibody (MilliporeSigma, A6154, 1:10000). One representative of three Western blots is shown in the figures.

NanoString nCounter expression analysis. Direct quantification of TRPV4 mRNA in murine lung cells was done as described previously (62). In brief, total RNA from pulmonary murine cells was isolated using the Qia RNeasy Mini Kit (QIAGEN). Quantity, purity, and integrity of the RNA samples were controlled by spectrophotometry (NanoQuant). Two probes (the reporter and the capture probe) were hybridized to their specific target mRNAs. Then, the target-probe complexes were immobilized in the imaging surface of the nCounter Cartridge by binding of the capture probe. Finally, the sample cartridges were scanned by an automated fluorescence microscope, and molecular barcodes (fluorophores contained in the reporter probe) for each specific target were counted. For expression analysis by nCounter NanoString technology, 200 ng total RNA was hybridized with a NanoString Gene Expression CodeSet and analyzed using the nCounter Digital Analyzer. Background correction was performed and normalization was applied using 4

JCI insight RESEARCH ARTICLE

Table 2. List of oligonucleotides used for nanostring nCounter expression analysis

Name	Primer sequence	Gene Id.
Primer pool A		
β-Actin	AAAAGAGCCTCAGGGCATCGGAACCGCTCGTTGCCAATAGT GATGACCTGCCTCAAGACCTAAGCGACAGCGTGACCTTGTTTCA	NM_007393.1:815
β2-Microglobulin	ATTTGGATTTCAATGTGAGGCGGGTGGAACTGTGTTACGTAGCA GTTCAGCATCCTCTTCTTTTCTTGGTGTTGAGAAGATGCTC	NM_009735.3:177
SdHa	GGCATGCAGTATTAAACCCTGCCTCAGAAAGGCCAAATG CAGCTCGCAAGCACAATTCTGCGGGTTAGCAGGAAGGTTAGGGAAC	NM_023281.1:250
GAPDH	ATCGAAGGTGGAAGAGTGGGAGTTGCTGTTGAAGTCGCA GGAGACAACCTCTGTTGAGATTATTGAGCTTCATCATGACCAGAAG	NM_001001303.1:890
TRPV4	GGCCTCGGTAGTAGATGTCTCTGAAGGGCGAGTTGAT GAATTCACGCATGCATAAAATTGGTTTTGCCTTTCAGCAATTCAACTT	NM_022017.3:776
Primer pool B		
β-Actin	CGAAAGCCATGACCTCCGATCACTCATGTAGTTT CATGGATGCCACAGGATTCCATACCCAAGAAGGAAGGCTGG	NM_007393.1:815
β2-Microglobulin	CGAAAGCCATGACCTCCGATCACTCAGGACATA TCTGACATCTCTACTTTAGGAATTTTTTTCCCGTTCTTCAGC	NM_009735.3:177
SdHa	CGAAAGCCATGACCTCCGATCACTCCTCCCTGTGCTGCA ACAGTATGTGATCGGGTAGGAAAGAGCTTTGTAA	NM_023281.1:250
GAPDH	CGAAAGCCATGACCTCCGATCACTCCAGGAAATGAGC TTGACAAAGTTGTCATTGAGAGCAATGCCAGCCCCGGC	NM_001001303.1:890
TRPV4	CGAAAGCCATGACCTCCGATCACTCCACGTAGTGCTTG CAGCGCCGTTCGATGGCAATGTGCAGGGATGTCT	NM_022017.3:776

SdHa, succinate dehydrogenase subunit A.

different housekeeping genes (succinate dehydrogenase subunit A [Sdha], β2-microglobulin, GAPDH, and β-actin). The DNA sequences used for mRNA expression analysis are summarized in Table 2.

Migration assay. Around 4.4×10^6 ATII cells/well were seeded on a 2-well silicone insert with a 500 μm cell-free gap (ibidi GmbH) and grown in DMEM (10% FCS, 1% HEPES, and 1% penicillin/streptomycin) for 5 days to obtain ATI-like cells. Subsequently, cells were starved in serum-reduced medium (0.1% FCS) for 24 hours before insert detachment to create a defined cell-free gap. Images were taken 0, 1, 3, 5, 8, 12, and 24 hours after gap creation. Migration was analyzed by measuring the remaining gap width with ImageJ software (NIH) in 3 images per time point and replicate.

Isolation of nuclear fractions. Isolation of nuclear protein extracts from ATI-like cells after 6 days of culture was performed with a Nuclear Extract Kit according to the manufacturer's instructions (Active Motif, 40010) as described previously (61). In brief, cells were first washed with PBS containing phosphatase inhibitors. Cytoplasmic protein fractions were collected by adding hypotonic lysis buffer and detergent, causing leakage of cytoplasmic proteins into the supernatant. After centrifugation (14,000*g* for 30 seconds), nuclear protein fractions were obtained by resuspending pellets in detergent-free lysis buffer containing protease inhibitors. NFAT proteins were analyzed by Western blotting as described below using an NFATc1-specific (mouse, Santa Cruz Biotechnology, sc-7294, 1:600) antiserum and lamin B1 (rabbit, Thermo Fisher Scientific, PA5-19468, 1:5000) antibodies as loading controls. Protein bands were normalized to loading controls and quantified by an Odyssey Fc unit (Licor).

Quantification of cell resistance by ECIS. Resistance changes of ATII cells differentiated to ATI cells were analyzed using an ECIS device (Applied Biophysics). Freshly isolated epithelial cells were seeded on ECIS culture ware (8W10E+; Applied Biophysics), which was preincubated with FCS for 3 hours and connected to the ECIS device. A total of 1×10^4 cells was seeded per chamber and grown at 37°C and 5% CO_2 in an incubator. Resistance (Ω) was analyzed at 2000 Hz over 160 hours.

Statistics. All statistical test were performed using GraphPad Prism 7. Numbers of mice and cells as well as statistical tests used are indicated in the figure legends and include 1-way ANOVA and 2-tailed unpaired Student's *t* test. A *P* value of less than 0.05 was considered significant.

Study approval. All animal experiments were approved by the local authority (Regierung Oberbayern, Munich, Germany).

Author contributions

JW and AD conceived the study, analyzed data, and wrote the manuscript. MB, NW, AÖY, JS, and CG aided in the experimental design. JW, YKC, CS, MK, GKC, and SR conducted the experiments. TG aided in critical analysis and in revising the manuscript. All authors read the manuscript and provided critical revisions.

Acknowledgments

The authors thank Bettina Braun for excellent technical assistance and the Riken BioResource Center (RBR) as well as the Mutant Mouse Resource and Research Center for providing the mouse models. This study was funded by the Deutsche Forschungsgemeinschaft (TRR 152, project 16 to AD, project 04 to CG, and project 22 to GKC; GRK 2338, project 04 to AD and project 08 to CG) and the DZL (to AD, MB, NW, and TG).

Address correspondence to: Alexander Dietrich, Walther-Straub-Institute of Pharmacology and Toxicology, Medical Faculty, LMU-Munich, Nussbaumstr. 26, 800336 Munich, Germany. Phone: 011.49.89.2180.73802; Email: alexander.dietrich@lrz.uni-muenchen.de.

1. Mutze K, Vierkotten S, Milosevic J, Eickelberg O, Königshoff M. Enolase 1 (ENO1) and protein disulfide-isomerase associated 3 (PDIA3) regulate Wnt/β-catenin-driven trans-differentiation of murine alveolar epithelial cells. *Dis Model Mech*. 2015;8(8):877–890.
2. Dobbs LG, Johnson MD, Vanderbilt J, Allen L, Gonzalez R. The great big alveolar TI cell: evolving concepts and paradigms. *Cell Physiol Biochem*. 2010;25(1):55–62.
3. Weibel ER. On the tricks alveolar epithelial cells play to make a good lung. *Am J Respir Crit Care Med*. 2015;191(5):504–513.
4. Stone KC, Mercer RR, Freeman BA, Chang LY, Crapo JD. Distribution of lung cell numbers and volumes between alveolar and nonalveolar tissue. *Am Rev Respir Dis*. 1992;146(2):454–456.
5. Fehrenbach H. Alveolar epithelial type II cell: defender of the alveolus revisited. *Respir Res*. 2001;2(1):33–46.
6. Halliday HL. Surfactants: past, present and future. *J Perinatol*. 2008;28 Suppl 1:S47–S56.
7. Desai TJ, Brownfield DG, Krasnow MA. Alveolar progenitor and stem cells in lung development, renewal and cancer. *Nature*. 2014;507(7491):190–194.
8. Hollenhorst MI, Richter K, Fronius M. Ion transport by pulmonary epithelia. *J Biomed Biotechnol*. 2011;2011:174306.
9. Nilius B, Szallasi A. Transient receptor potential channels as drug targets: from the science of basic research to the art of medicine. *Pharmacol Rev*. 2014;66(3):676–814.
10. Dietrich A, Steinritz D, Gudermann T. Transient receptor potential (TRP) channels as molecular targets in lung toxicology and associated diseases. *Cell Calcium*. 2017;67:123–137.
11. Hellwig N, Albrecht N, Harteneck C, Schultz G, Schaefer M. Homo- and heteromeric assembly of TRPV channel subunits. *J Cell Sci*. 2005;118(Pt 5):917–928.
12. Köttgen M, et al. TRPP2 and TRPV4 form a polymodal sensory channel complex. *J Cell Biol*. 2008;182(3):437–447.
13. Liedtke W, et al. Vanilloid receptor-related osmotically activated channel (VR-OAC), a candidate vertebrate osmoreceptor. *Cell*. 2000;103(3):525–535.
14. Strotmann R, Harteneck C, Nunnenmacher K, Schultz G, Plant TD. OTRPC4, a nonselective cation channel that confers sensitivity to extracellular osmolarity. *Nat Cell Biol*. 2000;2(10):695–702.
15. Hill-Eubanks DC, Gonzales AL, Sonkusare SK, Nelson MT. Vascular TRP channels: performing under pressure and going with the flow. *Physiology (Bethesda)*. 2014;29(5):343–360.
16. Marziano C, Hong K, Cope EL, Kotlikoff MI, Isakson BE, Sonkusare SK. Nitric oxide-dependent feedback loop regulates transient receptor potential vanilloid 4 (TRPV4) channel cooperativity and endothelial function in small pulmonary arteries. *J Am Heart Assoc*. 2017;6(12):e007157.
17. Lorenzo IM, Liedtke W, Sanderson MJ, Valverde MA. TRPV4 channel participates in receptor-operated calcium entry and ciliary beat frequency regulation in mouse airway epithelial cells. *Proc Natl Acad Sci USA*. 2008;105(34):12611–12616.
18. Li J, et al. TRPV4-mediated calcium influx into human bronchial epithelia upon exposure to diesel exhaust particles. *Environ Health Perspect*. 2011;119(6):784–793.
19. Henry CO, et al. In vitro and in vivo evidence for an inflammatory role of the calcium channel TRPV4 in lung epithelium: Potential involvement in cystic fibrosis. *Am J Physiol Lung Cell Mol Physiol*. 2016;311(3):L664–L675.
20. Goldenberg NM, Ravindran K, Kuebler WM. TRPV4: physiological role and therapeutic potential in respiratory diseases. *Naunyn Schmiedebergs Arch Pharmacol*. 2015;388(4):421–436.
21. Xia Y, et al. TRPV4 channel contributes to serotonin-induced pulmonary vasoconstriction and the enhanced vascular reactivity in chronic hypoxic pulmonary hypertension. *Am J Physiol, Cell Physiol*. 2013;305(7):C704–C715.
22. Goldenberg NM, Wang L, Ranke H, Liedtke W, Tabuchi A, Kuebler WM. TRPV4 is required for hypoxic pulmonary vasoconstriction. *Anesthesiology*. 2015;122(6):1338–1348.
23. Everaerts W, et al. Inhibition of the cation channel TRPV4 improves bladder function in mice and rats with cyclophosphamide-induced cystitis. *Proc Natl Acad Sci USA*. 2010;107(44):19084–19089.
24. Dietrich A. Modulators of transient receptor potential (TRP) channels as therapeutic options in lung disease. *Pharmaceuticals (Basel)*. 2019;12(1):E23.
25. Rahaman SO, et al. TRPV4 mediates myofibroblast differentiation and pulmonary fibrosis in mice. *J Clin Invest*. 2014;124(12):5225–5238.
26. Jian MY, King JA, Al-Mehdi AB, Liedtke W, Townsley MI. High vascular pressure-induced lung injury requires P450 epoxygenase-dependent activation of TRPV4. *Am J Respir Cell Mol Biol*. 2008;38(4):386–392.

27. Hamanaka K, et al. TRPV4 initiates the acute calcium-dependent permeability increase during ventilator-induced lung injury in isolated mouse lungs. *Am J Physiol Lung Cell Mol Physiol.* 2007;293(4):L923–L932.
28. Michalick L, Erfinanda L, Weichelt U, van der Giet M, Liedtke W, Kuebler WM. Transient receptor potential vanilloid 4 and serum glucocorticoid-regulated kinase 1 are critical mediators of lung injury in overventilated mice in vivo. *Anesthesiology.* 2017;126(2):300–311.
29. Thorneloe KS, et al. An orally active TRPV4 channel blocker prevents and resolves pulmonary edema induced by heart failure. *Sci Transl Med.* 2012;4(159):159ra148.
30. Akazawa Y, Yuki T, Yoshida H, Sugiyama Y, Inoue S. Activation of TRPV4 strengthens the tight-junction barrier in human epidermal keratinocytes. *Skin Pharmacol Physiol.* 2013;26(1):15–21.
31. Janssen DA, et al. TRPV4 channels in the human urogenital tract play a role in cell junction formation and epithelial barrier. *Acta Physiol (Oxf).* 2016;218(1):38–48.
32. Martínez-Rendón J, et al. TRPV4 regulates tight junctions and affects differentiation in a cell culture model of the corneal epithelium. *J Cell Physiol.* 2017;232(7):1794–1807.
33. Alvarez DF, King JA, Weber D, Addison E, Liedtke W, Townsley MI. Transient receptor potential vanilloid 4-mediated disruption of the alveolar septal barrier: a novel mechanism of acute lung injury. *Circ Res.* 2006;99(9):988–995.
34. Alpizar YA, et al. TRPV4 activation triggers protective responses to bacterial lipopolysaccharides in airway epithelial cells. *Nat Commun.* 2017;8(1):1059.
35. Balakrishna S, et al. TRPV4 inhibition counteracts edema and inflammation and improves pulmonary function and oxygen saturation in chemically induced acute lung injury. *Am J Physiol Lung Cell Mol Physiol.* 2014;307(2):L158–L172.
36. Steinritz D, Stenger B, Dietrich A, Gudermann T, Popp T. TRPs in Tox: Involvement of transient receptor potential-channels in chemical-induced organ toxicity-a structured review. *Cells.* 2018;7(8):E98.
37. Weissmann N, et al. Activation of TRPC6 channels is essential for lung ischaemia-reperfusion induced oedema in mice. *Nat Commun.* 2012;3:649.
38. Simmons S, Erfinanda L, Bartz C, Kuebler WM. Novel mechanisms regulating endothelial barrier function in the pulmonary microcirculation. *J Physiol (Lond).* 2019;597(4):997–1021.
39. Suzuki M, Mizuno A, Kodaira K, Imai M. Impaired pressure sensation in mice lacking TRPV4. *J Biol Chem.* 2003;278(25):22664–22668.
40. Mizuno A, Matsumoto N, Imai M, Suzuki M. Impaired osmotic sensation in mice lacking TRPV4. *Am J Physiol, Cell Physiol.* 2003;285(1):C96–101.
41. Kalwa H, et al. Phospholipase C epsilon (PLCε) induced TRPC6 activation: a common but redundant mechanism in primary podocytes. *J Cell Physiol.* 2015;230(6):1389–1399.
42. Mendoza SA, et al. TRPV4-mediated endothelial Ca2+ influx and vasodilation in response to shear stress. *Am J Physiol Heart Circ Physiol.* 2010;298(2):H466–H476.
43. Yin J, et al. Negative-feedback loop attenuates hydrostatic lung edema via a cGMP-dependent regulation of transient receptor potential vanilloid 4. *Circ Res.* 2008;102(8):966–974.
44. Suresh K, et al. Hydrogen peroxide-induced calcium influx in lung microvascular endothelial cells involves TRPV4. *Am J Physiol Lung Cell Mol Physiol.* 2015;309(12):L1467–L1477.
45. de Perrot M, Liu M, Waddell TK, Keshavjee S. Ischemia-reperfusion-induced lung injury. *Am J Respir Crit Care Med.* 2003;167(4):490–511.
46. Dobbs LG, Gonzalez R, Matthay MA, Carter EP, Allen L, Verkman AS. Highly water-permeable type I alveolar epithelial cells confer high water permeability between the airspace and vasculature in rat lung. *Proc Natl Acad Sci USA.* 1998;95(6):2991–2996.
47. Liu X, et al. A role for AQP5 in activation of TRPV4 by hypotonicity: concerted involvement of AQP5 and TRPV4 in regulation of cell volume recovery. *J Biol Chem.* 2006;281(22):15485–15495.
48. Sidhaye VK, Güler AD, Schweitzer KS, D'Alessio F, Caterina MJ, King LS. Transient receptor potential vanilloid 4 regulates aquaporin-5 abundance under hypotonic conditions. *Proc Natl Acad Sci USA.* 2006;103(12):4747–4752.
49. Hills BA. An alternative view of the role(s) of surfactant and the alveolar model. *J Appl Physiol.* 1999;87(5):1567–1583.
50. Pumiputavon K, et al. Cytotoxic and cytostatic effects of four Annonaceae plants on human cancer cell lines. *In Vitro Cell Dev Biol Anim.* 2019;55(9):723–732.
51. Ma T, Fukuda N, Song Y, Matthay MA, Verkman AS. Lung fluid transport in aquaporin-5 knockout mice. *J Clin Invest.* 2000;105(1):93–100.
52. King LS, Nielsen S, Agre P. Aquaporins and the respiratory system: advice for a lung investigator. *J Clin Invest.* 2000;105(1):15–16.
53. Yan C, Zhu Y, Zhang X, Chen X, Zheng W, Yang J. Down-regulated aquaporin 5 inhibits proliferation and migration of human epithelial ovarian cancer 3AO cells. *J Ovarian Res.* 2014;7:78.
54. Jiang XX, et al. Reduced migration of Ishikawa cells associated with downregulation of aquaporin-5. *Oncol Lett.* 2012;4(2):257–261.
55. Glasser SW, Detmer EA, Ikegami M, Na CL, Stahlman MT, Whitsett JA. Pneumonitis and emphysema in sp-C gene targeted mice. *J Biol Chem.* 2003;278(16):14291–14298.
56. Dietrich A, et al. Increased vascular smooth muscle contractility in TRPC6−/− mice. *Mol Cell Biol.* 2005;25(16):6980–6989.
57. Gong S, et al. A gene expression atlas of the central nervous system based on bacterial artificial chromosomes. *Nature.* 2003;425(6961):917–925.
58. John-Schuster G, et al. Cigarette smoke-induced iBALT mediates macrophage activation in a B cell-dependent manner in COPD. *Am J Physiol Lung Cell Mol Physiol.* 2014;307(9):L692–L706.
59. Corti M, Brody AR, Harrison JH. Isolation and primary culture of murine alveolar type II cells. *Am J Respir Cell Mol Biol.* 1996;14(4):309–315.
60. Dobbs LG. Isolation and culture of alveolar type II cells. *Am J Physiol.* 1990;258(4 Pt 1):L134–L147.
61. Hofmann K, et al. Classical transient receptor potential 6 (TRPC6) channels support myofibroblast differentiation and development of experimental pulmonary fibrosis. *Biochim Biophys Acta Mol Basis Dis.* 2017;1863(2):560–568.
62. Kannler M, Lüling R, Yildirim AÖ, Gudermann T, Steinritz D, Dietrich A. TRPA1 channels: expression in non-neuronal murine lung tissues and dispensability for hyperoxia-induced alveolar epithelial hyperplasia. *Pflugers Arch.* 2018;470(8):1231–1241.

4. Research paper II

Archives of Toxicology
https://doi.org/10.1007/s00204-022-03235-z

ORGAN TOXICITY AND MECHANISMS

An ex vivo perfused ventilated murine lung model suggests lack of acute pulmonary toxicity of the potential novel anticancer agent (−)-englerin A

Christian Schremmer[1] · Dirk Steinritz[2] · Thomas Gudermann[1] · David J. Beech[3] · Alexander Dietrich[1]

Received: 10 November 2021 / Accepted: 20 January 2022

Abstract
(−)-Englerin A (EA), a potential novel anti-cancer drug, is a potent selective activator of classical transient receptor potential 4 and 5 (TRPC4, TRPC5) channels. As TRPC4 channels are expressed and functional in the lung endothelium, possible side effects such as lung edema formation may arise during its administration. Well-established in vivo rodent models for toxicological testing, however, rapidly degrade this compound to its inactive derivative, englerin B. Therefore, we chose an ex vivo isolated perfused and ventilated murine lung (IPVML) model to detect edema formation due to toxicants, which also reduces the number of incriminating animal experiments required. To evaluate the sensitivity of the IPVML model, short-time (10 min) drops of the pH from 7.4 down to 4.0 were applied, which resulted in linear changes of tidal volumes, wet-to-dry weight ratios and incorporation of FITC-coupled dextran particles from the perfusate. As expected, biological activity of EA was preserved after perfusion in the IPVML model. Concentrations of 50–100 nM EA continuously perfused through the IPVML model did not change tidal volumes and lung weights significantly. Wet-to-dry weight ratios were increased after perfusion of 100 nM EA but permeation of FITC-coupled dextran particles from the perfusate to the lung tissues was not significantly different. Therefore, EA shows little or no significant acute pulmonary toxicity after application of doses expected to activate target ion channels and the IPVML is a sensitive powerful ex vivo model for evaluating acute lung toxicity in accordance with the 3R rules for animal experimentation.

Keywords Anti-cancer drug · Lung edema · Classical transient receptor potential 4 and 5 (TRPC4, TRPC5) · Tidal volume · Wet-to-dry weight ratio · FITC–dextran permeation assay

Abbreviations

$[Ca^{2+}]_i$	Intracellular Ca^{2+} concentration
EA	(−)-Englerin A
FITC	Fluorescein isothiocyanate
h	Hour(s)
IPVML	Isolated perfused and ventilated murine lung
min	Minute(s)
TRPC4/5	Classical transient receptor potential 4/5

✉ Alexander Dietrich
alexander.dietrich@lrz.uni-muenchen.de

[1] Walther Straub Institute of Pharmacology and Toxicology, Member of the German Center for Lung Research (DZL), Medical Faculty, LMU-Munich, Nussbaum Str. 26, 80336 Munich, Germany

[2] Bundeswehr Institute of Pharmacology and Toxicology, Neuherbergstraße 11, 80937 Munich, Germany

[3] School of Medicine, University of Leeds, LIGHT Building, Clarendon Way, Leeds LS2 9JT, England, UK

Introduction

(−)-Englerin A (EA) is a guaiane sesquiterpene originally isolated from the bark of the plant *phyllanthus engleri* from southern Africa (Wu et al. 2017). This natural product effectively inhibits growth of several kidney and breast cancer cell lines with an IC_{50} of 35–50 nM, while their non-tumorigenic counterparts were only affected at higher concentrations (> 10 µM) (Sourbier et al. 2013). Further analysis of cell lines revealed that EA is a potent activator of TRPC4 and TRPC5 channels and TRPC4 expression correlates with EA sensitivity of cancer cell lines (Akbulut et al. 2015; Carson et al. 2015). Both channels are members of the seven classical transient receptor potential family, which form homo- and heterotetrameric unselective cation channel. Death of synovial sarcoma (SW982) cells in vitro after application of EA (10 nM) occurs by Na^+ influx through TRPC1/4 heteromeric channels and is further increased by inhibition of Na^+/K^+-ATPase removing excess intracellular Na^+ ions (Ludlow

Published online: 14 February 2022

et al. 2017; Muraki et al. 2017). Application of EA (2 mg/kg body weight) resulted in a significant reduction in locomotor activity for about 1 h as a potential side effect (Cheung et al. 2018). TRPC4- and TRPC5-deficient mice were partially and TRPC4/5 double knock-out mice were fully protected from this adverse EA effect (Cheung et al. 2018). In contrast to TRPC1/5, TRPC1/4 channels were also detected in murine lung endothelium (Sundivakkam et al. 2012) and are responsible for thrombin-induced lung edema, which is reduced in TRPC4-deficient lungs (Tiruppathi et al. 2002). Analysis of pulmonary toxicity of EA, however, turned out to be complicated for two reasons. First, intravenous (IV) injection of EA doses of > 1 mg/kg body weight were lethal in rats and second EA was rapidly degraded with an estimated half time of ≈ 15 min into the inactive compound englerin B in mice and rats by serum esterases, but not in human serum (Carson et al. 2015). The authors observed labored breathing in mice after subcutaneous injection of EA (5 mg/kg body weight) (Carson et al. 2015). It was, however, unclear, if this side effect was due to EA, which never exceeded levels of 12 nM in blood, or its metabolite englerin B, which was rapidly detected after application in rodents but not in humans. Therefore, we employed a new ex vivo model for evaluating acute EA toxicity using the isolated, perfused and ventilated murine lung (IPVML) offering numerous advantages compared to an in vivo system. We hypothesized that due to the absence of esterase in the perfusate EA is not degraded and defined doses can be applied. Lung parameters are analyzed in real time during the experiment without high stress levels in a living mouse. Moreover, wet to dry weight ratios and invasion of perfused fluorescein isothiocyanate (FITC)–dextran particle in the lung tissue can be quantified after the experiment. The applicability of the model was evaluated after applying short-time graduated pH changes from pH 7.4 to pH 4.0, which resulted in significant linear changes of values for wet-to-dry ratios and tidal volumes. Most interestingly, EA showed no significant changes in lung parameters and edema formation upon application of 50 or 100 nM EA [fivefold or tenfold of the EC_{50} values obtained in vitro experiments with SW982 cells (Muraki et al. 2017)] in comparison to control mice receiving electrolyte solution only.

Materials and methods

Chemicals

Electrolyte solution was prepared by the Apotheke Klinikum der Universität München: 7.19 g sodium chloride, 0.33 g potassium chloride, 0.27 g magnesium hexahydrate, 0.36 g calcium chloride dihydrate, 0.15 g potassium dihydrogen orthophosphate, 2.67 g glucose monohydrate, 51.28 g hydroxyethyl starch 200000/05 ad 1000 ml with aqua ad injectabilia, use 0.1848 mg/ml sodium hydrogen carbonate to adjust pH to 7.4. (−)-Englerin A (EA) was purchased from Roth (6492.1, Karlsruhe, Germany), Fluorescein isothiocyanate was provided from Sigma (90718, average Mw 70 kD, Taufkirchen, Germany) and GeneJuice® Transfection Reagent was ordered from Sigma (70967, Taufkirchen, Germany). EA stock solution was prepared at 100 mM in the Novartis approved standard solution for all in-life preclinical evaluations containing 5% ethanol, 10% polyethylene glycol 300 (Sigma Aldrich), 5% cremophor EL (Merck Chemicals Ltd), and 80% PBS as described before (Carson et al. 2015; Cheung et al. 2018). The final concentration of this solution was 0.0001% in the electrolyte buffer.

Isolated perfused and ventilated murine lung (IPVML)

IPVML were prepared from C57BL/6 mice as described previously (Weissmann et al. 2006, 2012). Mice were anesthetized and anticoagulated by i.p. injection of ketamine (100 mg/kg body weight (bw), Covetrus, Hamburg, Germany), xylazine (7 mg/kg bw, Covetrus, Hamburg, Germany) and with heparin (500 U/kg bw, Meditech Vertriebs GmbH, Parchim, Germany). Lungs were transferred from the body into an artificial glass thorax, ventilated with room air (positive pressure ventilation, 90 breath/min) and perfused with the blood-free electrolyte solution heated to 37 °C. Upon reaching a final flow rate of 2 ml/min ventilation was switched to negative pressure (90 breath/min, 50% inspiration time) and a deep inspiration was initiated every 5 min. After 15 min of perfusion, an external reservoir (20 ml) containing electrolyte solution and indicated compounds (pH drop or EA) was connected and after an additional 4 min the perfusion circuit, which then contained only perfusion solution of the external reservoir, was closed. The pH was continuously measured in the external reservoir and adjusted, if necessary, in the first 10 min by a pH meter (WTW inoLab® pH 7110, Weilheim, Germany). All data were transmitted to a computer and constantly monitored with the Pulmodyn software (Hugo Sachs Elektronik, March-Hugstetten, Germany). During perfusion with FITC–dextran particles, the solution was protected from light to avoid bleaching.

Wet-to-dry weight ratios

For wet-to-dry weight ratios lung weight was quantified directly after the experiment (wet weight) and after drying at 50 °C for 48 h (dry weight).

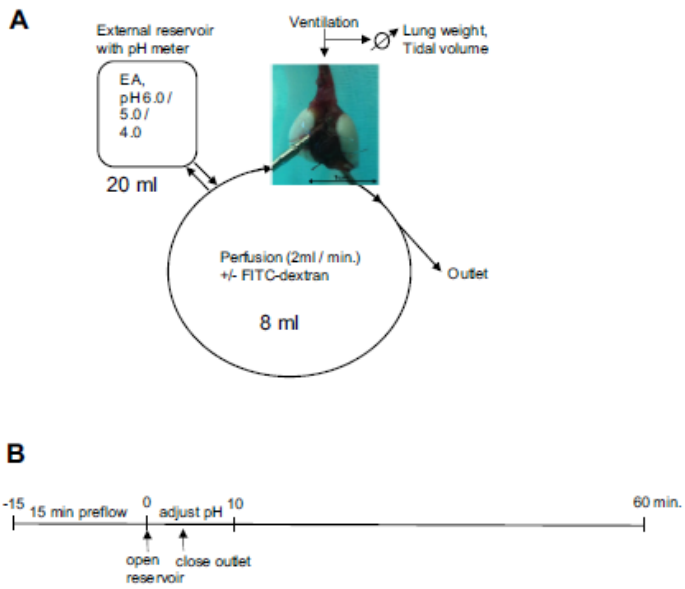

Fig. 1 Experimental setup of the isolated perfused ventilated murine lung (IPVML) model (**A**). A freshly isolated lung heart preparation was perfused through the pulmonary artery and ventilated through the trachea. Twenty ml of solutions with Englerin A (EA, 50, 100 nM) or equilibrated to pH 6.0, pH 5.0 and pH 4.0 were relased from a reservoir in the perfusion solution. Lung weight and tidal volumes were continously quantified by in built weighing scales or the software, respectively. Time line of the experiment (**B**). After 15 min perfusion EA in solution or solutions of decreased pH were released from the reservoir. The pH was continously measured in the reservoir and adjusted for 10 min, if necessary. The outlet was closed after 4 min and the perfusion solutions circulated for another 50 min in a closed circuit

Ca^{2+} imaging

HEK293T cells were grown on Ø 25 mm coverslips for 24 h and transfected with a TRPC4β1 cDNA in a pIRES2 plasmid containing an eGFP cDNA under the control of the internal ribosome entry site (IRES) using GeneJuice® solution as described by the manufacturer for 24 h. Cells were washed and loaded with FURA-2-AM (2 µM, F0888, Sigma, Taufkirchen, Germany) in 0,1% BSA in HEPES buffered HBSS at 37 °C for 30 min. Coverslips were washed with HEPES buffered HBSS and placed under a microscope in a recording chamber with a 500 µl volume. An increase in intracellular Ca^{2+} was recorded using a Leica DFC9000 GT camera coupled to an inverted microscope (DMi8, Leica, Wetzlar, Germany) with an 40x/0.85 oil immersions objective at 340 and 380 nm for quantification of $[Ca^{2+}]_i$ as described (Bendiks et al. 2020).

Lung histology

Following perfusion with FITC–dextran particles mouse lungs were incubated in 4% (w/v) paraformaldehyde in PBS and processed for embedding in O.C.T™ Compound (Tissue-Tek®, Sakura Finetek, Umkirch, Germany) as described before (Weber et al. 2020). Cryo-embedded lungs were cut in 10 µm sections using a cryotome (CM1900, Leica, Wetzlar, Germany) and mounted on glass slides in Dako Omnis Fluorescence mounting medium (GM30411-2, Agilent Technologies, Santa Clara, USA). Lung sections were analyzed using both a confocal microscope (LSM 880, Carl Zeiss Jena, Germany) and a fluorescence scanner (Typhoon Trio, GE Healthcare, Solingen, Germany).

Data analysis

Data analysis was performed using R and data were plotted using GraphPad Prism 9. Used statistical tests and p values are indicated in the figure legends.

Results

Experimental setup for detection of acute lung toxicity by ex vivo isolated perfused ventilated murine lungs (IPVML)

The experimental setup and the timeline for the detection of acute lung toxicity in the IPVML by edema formation are depicted in Fig. 1A, B, respectively. After mounting, a freshly isolated murine lung was ventilated and perfused with an open outlet for 15 min. A 20 ml reservoir containing the substance to be tested [EA (50, 100 nM)) or

perfusion solution of decreased pH values (pH 6.0, 5.0 and 4.0)] replaced the perfusion solution and pH values were adjusted for 10 min in the external reservoirs. The outlet was closed and lungs were continuously perfused with or without FITC–dextran particles and monitored for an additional 50 min. Lung weight and tidal volume were constantly quantified during the experiment, while wet-to-dry weight ratios and invasion of FITC–dextran particles in the tissues were analyzed after the experiment.

Validation of the IPVML for detection of acute lung toxicity induced by short drops of the pH

To evaluate the sensitivity of the IPVML model, we applied solutions with a decreased pH (pH 6.0, pH 5.0 and pH 4.0). Significant increases in lung weight due to an acute formation of lung edema during the experiment were only detected for a short-time drop to pH 4.0, but not for pH 5.0 or pH 6.0 (Fig. 2A). A linear decrease in tidal volumes with dropping pH values was, however, obvious during the experiment (Fig. 2B). Wet-to-dry weight ratios after the experiment were linearly increased for transient drops to pH 6.0, pH 5.0 and pH 4.0 (Fig. 2C). Therefore, short-time changes in pH correlate with a linear increase in wet-to-dry weight ratios and a linear decrease in tidal volumes in the IVPML model. The experimental setup is, therefore, suitable and sensitive enough to detect acute lung edema in a linear fashion.

Biological activity of (−)-englerin A (EA) before and after perfusion in the IPVML

The biological activity of EA (Fig. 3A) was quantified by Ca^{2+} imaging of HEK 293T cells heterologously expressing TRPC4 channels after transfection with a pIRES plasmid carrying cDNAs for TRPC4 and an enhanced green fluorescent protein (eGFP). EA (50 and 100 nM) before and after the experiment (1 h perfusion) was able to increase intracellular Ca^{2+} ($[Ca^{2+}]_i$) levels by opening TRPC4 channels and Ca^{2+}-influx through the channel pore, while non-transfected cells show only minor changes in $[Ca^{2+}]_i$ (Fig. 3B–E). Our results indicate a preserved biological activity of EA after 1 h perfusion in the IPVML model.

Evaluation of acute lung toxicity induced by EA in the IPVML

Changes in lung weight during 1 h perfusion of EA (50 and 100 nM) in comparison to electrolyte solution are depicted in Fig. 4A. No significant differences were observed. The same was true for the analysis of tidal volumes during the experiment (Fig. 4B). Wet-to-dry weight ratios showed, in comparison to short drops in pH, a small but significant

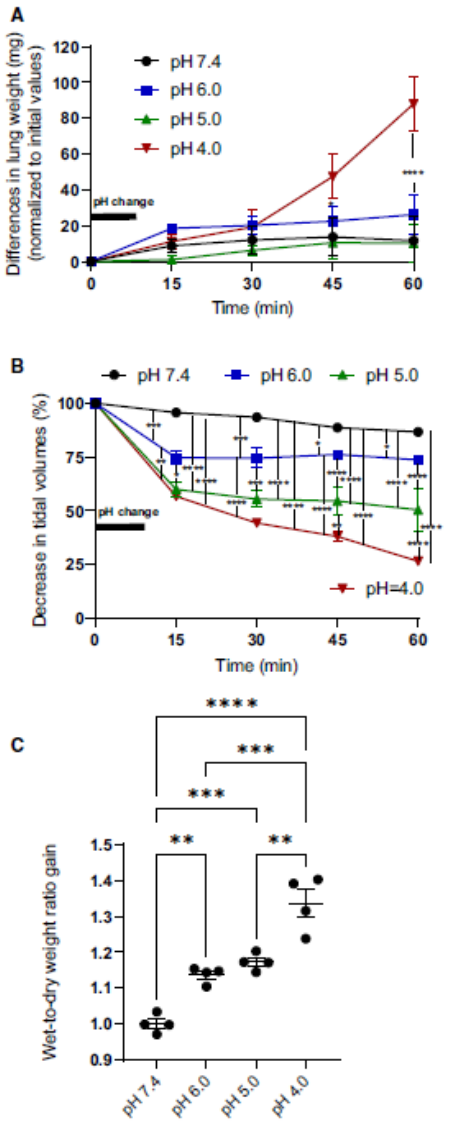

Fig. 2 Lung weight gain after a short (10 min) drop of the pH to 6.0, 5.0 and 4.0 (**A**). Changes in tidal volumes after a short (10 min) drop of the pH to 6.0, 5.0 and 4.0 (**B**). Increases in wet-to-dry weight ratios after a short (10 min) drop of the pH to 6.0, 5.0 and 4.0 were quantified after the experiment (**C**). Data are means ± SEM. *p* values were calculated by two way ANOVA and are indicated by asterisks (*, $p<0.05$; 2*, $p<0.01$; 3*, $p<0.001$, 4*, $p<0.0001$)

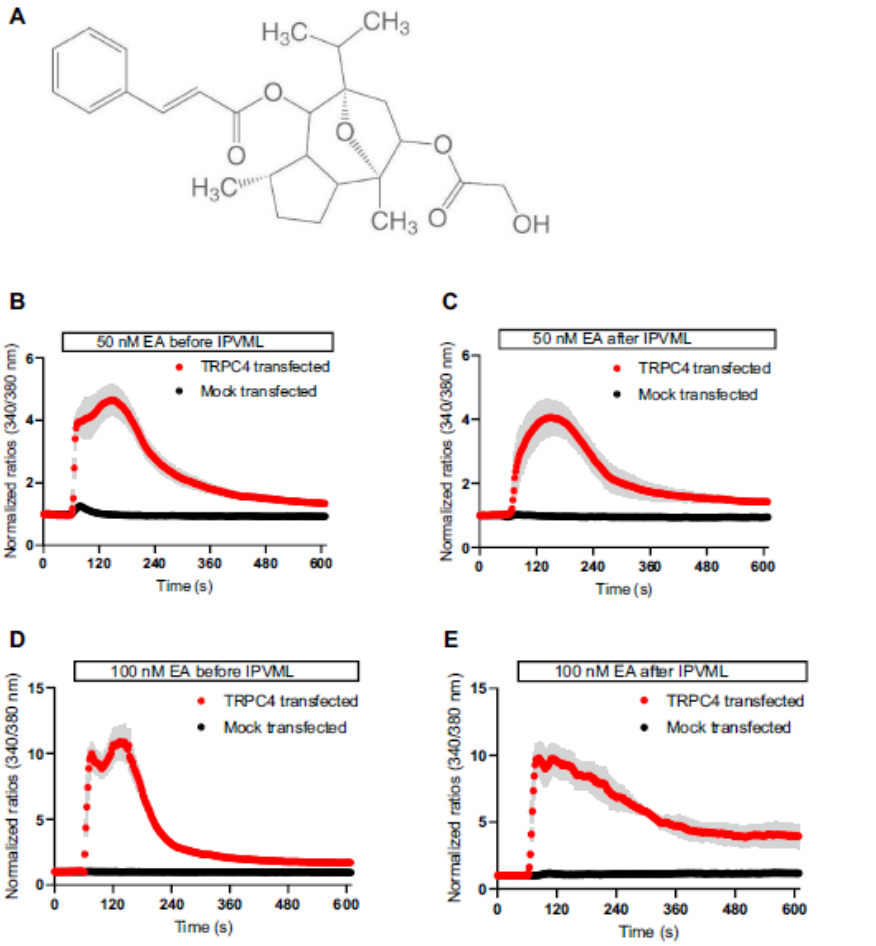

Fig. 3 Structural formula of (−)-englerin A (EA, provided by the manufacturer, see www.carlroth.com, **A**) and Ca^{2+} imaging experiments of HEK 293T cells heterologously expressing TRPC4 channels (TRPC4 transfected) or mock-transfected controls after application of EA (50 nM, 100 nM) before and after 1 h perfusion in the IPVLM model. One representative experiment (n > 3 cells) out of three is shown (**B–E**)

increase after application of EA (100 nM), which was not detectable for the lower concentration (50 nM) (Fig. 4C).

Quantification of lung permeability by tissue permeation of FITC–dextran particles in the IPVML

Endothelial and tissue permeabilty is significantly increased after exposure of toxicants from the vascular side. To quantify tissue permeation of liquids and invading cells fluorescein isothiocyanate (FITC)-coupled dextran particles

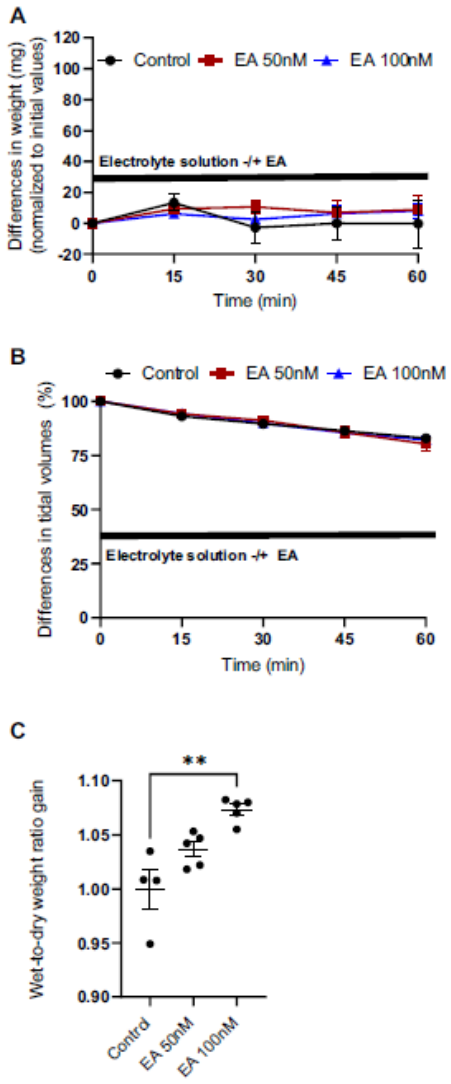

Fig. 4 Lung weight gain after application of (−)-englerin A (EA, 50 and 100 nM) (**A**). Changes in tidal volumes after application of EA (50 and 100 nM) (**B**). Increases in wet-to-dry weight ratios after after application of EA (50 and 100 nM) (**C**). Data are means + SEM. *p* values were calculated by two way ANOVA and are indicated by asterisks (*, $p<0.05$; 2*, $p<0.01$)

are used in cell biology and in vivo animal experiments (Thorball 1981). To test if our model is also able to detect increases in tissue permeabilty in a linear fashion, we added FITC–dextran particles in the perfusion solution during the preflow and analysed whole lungs by confocal laser scanning microscopy and by a laser scanning platform. Tissues after a short drop to pH 4.0 incorporated a significant higher amount of FITC–dextran particle than tissues perfused with control solution of a pH 7.4 as shown in overlay images in Fig. 5A. To quantify fluorescence in tissues without a selection bias, we scanned whole lungs on a laser scanning platform as shown in Fig. 5B. Integrated fluorescent values normalized to values of non-perfused lungs are shown in Fig. 5C. Short-time pH drops caused a significant linear increase in incorporation of FITC–dextran particels compared to EA and electrolyte solution-only perfused mouse lungs. Therefore, this ex vivo lung model is also suitable to detect higher tissue permeability after application of toxicants by permeation of FITC–dextran particles.

Discussion

EA is a promising anti-cancer compound inhibiting tumor growth of several kidney (Ratnayake et al. 2009) (Akbulut et al. 2015), breast cancer (Grant et al. 2019) and synovial carcinoma cell lines (Muraki et al. 2017). Its toxicological evaluation in rodents, however, is complicated for two reasons. Intravenous injections of EA (2 mg/kg body weight) were lethal to rats and after subcutaneous application EA was rapidly degraded into the inactive englerin B in mice and rats, while it remains stable in humans (Carson et al. 2015). Therefore, we choose the IPVML model as an ex vivo approach to evaluate acute pulmonary toxicity of EA independently from the mode of application and degradation. We first tested its sensitivity by short drops of the pH of the perfusion medium from pH 7.4 to pH 4.0. These pH changes can be observed in asthma patients after accumulation of CO_2 in their blood due to their inability to exhale or by infusion of acids (Richardson et al. 1961). Moreover, metabolic acidosis and septic shock also decrease pH values in the blood (Mizock and Falk 1992). Significant linear increases were observed for wet-to-dry weight ratios (Fig. 2C), while tidal volumes decreased (Fig. 2B) after a stepwise drop in pH to 4.0. Lung edema formation quantified by an increase in lung weight during perfusion and ventilation were only detected after a drop to pH 4.0, while decreases to pH 5.0 and 6.0 did not induce immediate changes in lung weight (Fig. 2A). While small drops in pH to 6.5 did not change intracellular pH values significantly in endothelial cells of the rat aorta but increase intracellular NO concentrations (Capellini et al. 2013), large decreases in pH values may damage endothelial cells and increases endothelial

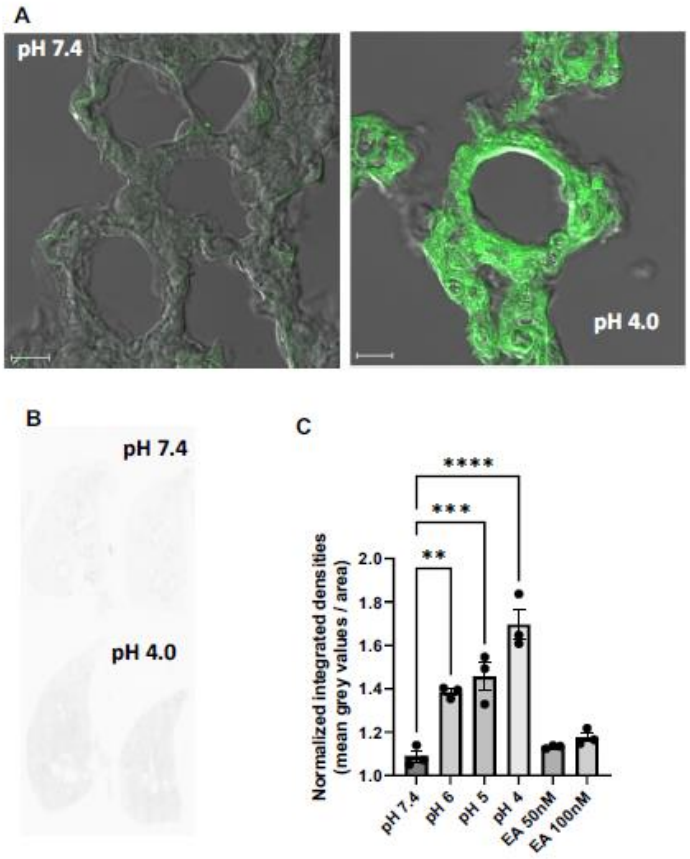

Fig. 5 Tissue permeation of fluorescein isothiocyanate (FITC) dextrane particle after perfusion of lungs at pH 7.4 and after a short (10 min) drop of the pH to 4.0. Two representative overlays of FITC fluorescence and coresponding differential interference contrast (DIC) images showing lung tissues after perfusion of electrolyte solution (pH 7.4) and after a short (10 min) drop in pH (pH 4.0) are depicted (**A**). Two representative scans from total lungs at pH 7.4 and after a short (10 min) drop of the pH to 4.0 (**B**). Normalized integrated densities of lungs after a short (10 min) drop of the pH to 6.0, 5.0 and 4.0 or perfused with EA (50 and 100 nM) were normalized to lungs perfused with electrolyte solution at pH 7.4 and plotted as columns. Data are means ± SEM. p values were calculated by two way ANOVA and are indicated by asterisks (*, $p < 0.05$)

permeability. As a consequence flooding of alevoli by protein rich fluid, increases lung weight and reduces tidal volumes. Therefore, the ex vivo IPVML model realistically maps the in vivo situation of acute lung toxicity by quantifying edema formation due to a transient decreased pH.

The biological activity of EA was tested before and after 1 h perfusion in the IPVML model by application to HEK 293T cells heterologously expressing TRPC4 channels or control cells. EA induced significant increases in $[Ca^{2+}]_i$ as already described (Akbulut et al. 2015) even after 1 h of perfusion in the IPVML model in comparison to control cells (Fig. 3A–D). As expected EA is still active and supposedly not degraded to the inactive englerin B in our perfusion solution as enzymes, such as esterases, which might degrade EA in rodents in vivo (Carson et al. 2015), may not be present in the IPVML model.

Tidal volumes and lung weights correlating with lung edema formation were not changed during the experiment (Fig. 4A, B) using EA for perfusion in concentrations of 50 and 100 nM, while wet-to-dry weight ratios after the experiments were significantly increased after application of 100 nM EA (Fig. 4C).

However, histological analysis of lung sections after perfusion with FITC–dextran particle revealed a similar linear increase in the incorporation of these particles in the lung tisues by transient drops of the pH, while both concentrations of EA were not able to change fluorescence intensities significantly (Fig. 5C). Therefore, a significant change in edema formation as detected in wet-to-dry weight ratios

after perfusion with 100 nM EA was not confirmed in these experiments.

An overall comparison of the parameters collected in the IPVML model places tidal volumes, wet-to-dry weight ratios and FITC–dextran tissue distribution as the most sensitive values for detection of acute lung toxicity after a short pH drop, while lung weight changes during perfusion were only able to detect a major change in pH from 7.4 to 4.0.

In light of an expression of TRPC4 channels in the lung endothelium and their identified ability to increase endothelial permeabilty after activation of protease-activated receptors (PAR) by thrombin (Tiruppathi et al. 2002), our results with the highly specific TRPC4 activator EA are somewhat surprising. Except for changes in the wet-to-dry weight ratios after perfusion with 100 nM EA, we detected no differences in edema formation after application of EA in comparison to electrolyte solution as control. This discrepancy may be due to a close clustering of PAR together with TRPC4 channels in calveolar, such as compartments, which are not easily accessible for EA from the perfusate. This hypothesis needs to be further studied in the future.

In summary, the IPVML model is suitable to evaluate acute pulmonary toxicity of drug candidates by quantification of lung edema formation independently of drug application and metabolism. In the future numerous already established gene-deficient mouse models may also be used to identify toxicant sensors in the lung by this method. Moreover, this ex vivo model eliminates stress in mice after in vivo application of drugs and is, therefore, an important refinement according to the 3R ethical guidelines of animal experimentation.

Acknowledgements The authors thank Bettina Braun and Astrid Bauer for excellent technical assistance and are grateful to Dr. Ursula Storch, Aaron Treder and Christian Hermann for providing the TRPC4 eGFP IRES plasmid as well as for help with the transfection experiments.

Author contributions All authors contributed to the study conception and design. Material preparation, data collection and analysis were performed by Christian Schremmer and Alexander Dietrich. The first draft of the manuscript was written by Alexander Dietrich and all authors commented on previous versions of the manuscript. All authors read and approved the final manuscript.

Funding Open Access funding enabled and organized by Projekt DEAL. This work was supported by the Deutsche Forschungsgemeinschaft (DFG, Research Training Group GRK 2338).

Declarations

Conflict of interest David Beech is an inventor on a patent to develop EA analogues as anti-cancer therapeutics: U.S. Patent No. 11,098,054 issued August 24, 2021. This patent can remain in force until July 5, 2038. Compounds for Treating Cancer. Inventors: John Beutler, Antonio Echavarren, William Chain, David Beech, Zhenhua Wu, Jean-Simon Suppo, Fernando Bravo, Hussein Rubaiy.The other authors declare no conflict of interest.

Ethical standards All animal experiments were approved by the local authority (Regierung Oberbayern) and are, therefore, been performed in accordance with the ethical standards laid down in the 1964 Declaration of Helsinki and its later amendments.

References

Akbulut Y, Gaunt HJ, Muraki K et al (2015) (−)-Englerin A is a potent and selective activator of TRPC4 and TRPC5 calcium channels. Angew Chem Int Ed Engl 54(12):3787–3791. https://doi.org/10.1002/anie.201411511

Bendiks L, Geiger F, Gudermann T, Feske S, Dietrich A (2020) Store-operated Ca(2+) entry in primary murine lung fibroblasts is independent of classical transient receptor potential (TRPC) channels and contributes to cell migration. Sci Rep 10(1):6812. https://doi.org/10.1038/s41598-020-63677-2

Capellini VK, Restini CB, Bendhack LM, Evora PR, Celotto AC (2013) The effect of extracellular pH changes on intracellular pH and nitric oxide concentration in endothelial and smooth muscle cells from rat aorta. PLoS ONE 8(5):e62887. https://doi.org/10.1371/journal.pone.0062887

Carson C, Raman P, Tullai J et al (2015) Englerin A agonizes the TRPC4/C5 cation channels to inhibit tumor cell line proliferation. PLoS ONE 10(6):e0127498. https://doi.org/10.1371/journal.pone.0127498

Cheung SY, Henrot M, Al-Saad M et al (2018) TRPC4/TRPC5 channels mediate adverse reaction to the cancer cell cytotoxic agent (−)-Englerin A. Oncotarget 9(51):29634–29643. https://doi.org/10.18632/oncotarget.25659

Grant CV, Carver CM, Hastings SD et al (2019) Triple-negative breast cancer cell line sensitivity to englerin A identifies a new, targetable subtype. Breast Cancer Res Treat 177(2):345–355. https://doi.org/10.1007/s10549-019-05324-7

Ludlow MJ, Gaunt HJ, Rubaiy HN et al (2017) (−)-Englerin A-evoked cytotoxicity is mediated by Na+ influx and counteracted by Na+/K+-ATPase. J Biol Chem 292(2):723–731. https://doi.org/10.1074/jbc.M116.755678

Mizock BA, Falk JL (1992) Lactic acidosis in critical illness. Crit Care Med 20(1):80–93. https://doi.org/10.1097/00003246-199201000-00020

Muraki K, Ohnishi K, Takezawa A et al (2017) Na(+) entry through heteromeric TRPC4/C1 channels mediates (−)Englerin A-induced cytotoxicity in synovial sarcoma cells. Sci Rep 7(1):16988. https://doi.org/10.1038/s41598-017-17303-3

Ratnayake R, Covell D, Ransom TT, Gustafson KR, Beutler JA (2009) Englerin A, a selective inhibitor of renal cancer cell growth, from *Phyllanthus engleri*. Org Lett 11(1):57–60. https://doi.org/10.1021/ol802339w

Richardson DW, Wasserman AJ, Patterson JL Jr (1961) General and regional circulatory responses to change in blood pH and carbon

dioxide tension. J Clin Invest 40:31–43. https://doi.org/10.1172/JCI104234

Sourbier C, Scroggins BT, Ratnayake R et al (2013) Englerin A stimulates PKCtheta to inhibit insulin signaling and to simultaneously activate HSF1: pharmacologically induced synthetic lethality. Cancer Cell 23(2):228–237. https://doi.org/10.1016/j.ccr.2012.12.007

Sundivakkam PC, Freichel M, Singh V et al (2012) The Ca(2+) sensor stromal interaction molecule 1 (STIM1) is necessary and sufficient for the store-operated Ca(2+) entry function of transient receptor potential canonical (TRPC) 1 and 4 channels in endothelial cells. Mol Pharmacol 81(4):510–526. https://doi.org/10.1124/mol.111.074658

Thorball N (1981) FITC-dextran tracers in microcirculatory and permeability studies using combined fluorescence stereo microscopy, fluorescence light microscopy and electron microscopy. Histochemistry 71(2):209–233. https://doi.org/10.1007/BF00507826

Tiruppathi C, Freichel M, Vogel SM et al (2002) Impairment of store-operated Ca2+ entry in TRPC4(-/-) mice interferes with increase in lung microvascular permeability. Circ Res 91(1):70–76

Weber J, Rajan S, Schremmer C et al (2020) TRPV4 channels are essential for alveolar epithelial barrier function as protection from lung edema. JCI Insight. https://doi.org/10.1172/jci.insight.134464

Weissmann N, Dietrich A, Fuchs B et al (2006) Classical transient receptor potential channel 6 (TRPC6) is essential for hypoxic pulmonary vasoconstriction and alveolar gas exchange. Proc Natl Acad Sci USA 103(50):19093–19098

Weissmann N, Sydykov A, Kalwa H et al (2012) Activation of TRPC6 channels is essential for lung ischaemia-reperfusion induced oedema in mice. Nat Commun 3:649. https://doi.org/10.1038/ncomms1660

Wu Z, Zhao S, Fash DM, Li Z, Chain WJ, Beutler JA (2017) Englerins: a comprehensive review. J Nat Prod 80(3):771–781. https://doi.org/10.1021/acs.jnatprod.6b01167

References

1. West, J.B., *Comparative physiology of the pulmonary blood-gas barrier: the unique avian solution.* Am J Physiol Regul Integr Comp Physiol, 2009. **297**(6): p. R1625-34.
2. Hogan, B. and P.R. Tata, *Cellular organization and biology of the respiratory system.* Nat Cell Biol, 2019.
3. Matthys, H. and W. Seeger, *Klinische Pneumologie*. Vol. 4. 2008.
4. Volckaert, L. and S. De Langhe, *Lung epithelial stem cells and their niches: Fgf10 takes center stage.* Fibrogenesis & Tissue Repair, 2014. **7**(8).
5. Stone, K.C., et al., *Allometric Relationships of Cell Numbers and Size in the Mammalian Lung.* American Journal of Respiratory Cell and Molecular Biology, 1992. **6**: p. 235-243.
6. Dobbs, L.G., et al., *Highly water-permeable type 1 alveolar epithelial cells confer high water permeability between the airspace and vasculature in rat lung.* PNAS, 1998. **95**: p. 2991-2996.
7. Dobbs, L.G.J., M. D.; Vanderbilt, J.; Allen, L.; Gonzalez, R., *The Great Big Alveolar TI Cell: Evolving Concepts and Paradigms.* Cellular Physiology and Biochemistry, 2010. **25**: p. 55-62.
8. Avery, M.E. and J. Mead, *Surface Properties in Relation to Atelectasis and Hyaline Membrane Disease.* American Journal of Diseases of Children, 1959. **97**: p. 517-523.
9. Rock, J.R., et al., *Multiple stromal populations contribute to pulmonary fibrosis without evidence for epithelial to mesenchymal transition.* Proc Natl Acad Sci U S A, 2011. **108**(52): p. E1475-83.
10. White, E.S., *Lung extracellular matrix and fibroblast function.* Ann Am Thorac Soc, 2015. **12 Suppl 1**: p. S30-3.
11. Organization, W.H. *The top 10 causes of death*. 2020 21.03.2022]; Available from: https://www.who.int/news-room/fact-sheets/detail/the-top-10-causes-of-death.
12. Cui, X., et al., *Pulmonary Edema in COVID-19 Patients: Mechanisms and Treatment Potential.* Front Pharmacol, 2021. **12**: p. 664349.
13. Powell, J.G., D.; O'Reilly, S.; Punton, G., *Acute pulmonary edema.* Nursing Standard, 2016. **30**(23): p. 51-59.
14. Pappas, L. and G. Filippatos, *Pulmonary Congestion in Acute Heart Failure: From Hemodynamics to Lung Injury and Barrier Dysfunction.* Revista Española de Cardiología (English Edition), 2011. **64**(9): p. 735-738.
15. Ware, L.B.M., M. A., *Acute Pulmonary Edema.* New England Journal of Medicine, 2005. **353**: p. 2788-2796.
16. Nugent, K., et al., *Lung morphology and surfactant function in cardiogenic pulmonary edema: a narrative review.* J Thorac Dis, 2019. **11**(9): p. 4031-4038.
17. McMurray, J.J.V. and M.A. Pfeffer, *Heart failure.* The Lancet, 2005. **365**(9474): p. 1877-1889.
18. Abubacker, A.P., et al., *Non-invasive Positive Pressure Ventilation for Acute Cardiogenic Pulmonary Edema and Chronic Obstructive Pulmonary Disease in Prehospital and Emergency Settings.* Cureus, 2021. **13**(6): p. e15624.
19. Muller-Redetzky, H.C., et al., *Increasing the inspiratory time and I:E ratio during mechanical ventilation aggravates ventilator-induced lung injury in mice.* Crit Care, 2015. **19**: p. 23.
20. Dushianthan, A., et al., *Acute respiratory distress syndrome and acute lung injury.* Postgrad Med J, 2011. **87**(1031): p. 612-22.
21. de Leeuw, P.W. and A. Dees, *Fluid homeostasis in chronic obstructive lung disease.* Eur Respir J Suppl, 2003. **46**: p. 33s-40s.
22. Bolaki, M. and K.M. Antoniou, *Combined Pulmonary Fibrosis and Emphysema.* Semin Respir Crit Care Med, 2020. **41**(2): p. 177-183.
23. Dietrich, A., *Modulators of Transient Receptor Potential (TRP) Channels as Therapeutic Options in Lung Disease.* Pharmaceuticals (Basel), 2019. **12**(1).

24. Dietrich, A., *Transient Receptor Potential (TRP) Channels in Health and Disease.* Cells, 2019. **8**(5).

25. Zergane, M., W.M. Kuebler, and L. Michalick, *Heteromeric TRP Channels in Lung Inflammation.* Cells, 2021. **10**(7).

26. Hofmann, K., et al., *Classical transient receptor potential 6 (TRPC6) channels support myofibroblast differentiation and development of experimental pulmonary fibrosis.* Biochim Biophys Acta Mol Basis Dis, 2017. **1863**(2): p. 560-568.

27. Tiruppathi, C., et al., *Impairment of store-operated Ca2+ entry in TRPC4(-/-) mice interferes with increase in lung microvascular permeability.* Circ Res, 2002. **91**(1): p. 70-6.

28. Grune, J., A. Tabuchi, and W.M. Kuebler, *Alveolar dynamics during mechanical ventilation in the healthy and injured lung.* Intensive Care Med Exp, 2019. **7**(Suppl 1): p. 34.

29. Jaffal, S.M. and M.A. Abbas, *TRP channels in COVID-19 disease: Potential targets for prevention and treatment.* Chem Biol Interact, 2021. **345**: p. 109567.

30. Clapham, D.E., *Calcium Signaling.* Cell, 1995. **80**: p. 259-268.

31. Gees, M., B. Colsoul, and B. Nilius, *The role of transient receptor potential cation channels in Ca2+ signaling.* Cold Spring Harb Perspect Biol, 2010. **2**(10): p. a003962.

32. Montell, C., *Physiology, Phylogeny, and Functions of the TRP Superfamily of Cation Channels.* Science Signaling, 2001. **90**.

33. Rohacs, T., et al., *PI(4,5)P2 regulates the activation and desensitization of TRPM8 channels through the TRP domain.* Nat Neurosci, 2005. **8**(5): p. 626-34.

34. Gregorio-Teruel, L., et al., *The Integrity of the TRP Domain Is Pivotal for Correct TRPV1 Channel Gating.* Biophys J, 2015. **109**(3): p. 529-41.

35. Phelps, C.B., et al., *Insights into the roles of conserved and divergent residues in the ankyrin repeats of TRPV ion channels.* Channels (Austin), 2007. **1**(3): p. 148-51.

36. Phelps, C.B., et al., *Structural Anlysis of the Ankyrin Repeat Domain of TRPV6 and Related TRPV Ion Channels.* Biochemistry, 2008. **47**(8): p. 2476-2484.

37. Caterina, M.J., et al., *The capsaicin receptor: a heat-activated ion channel in the pain pathway.* Nature, 1997. **389**: p. 816-824.

38. Goldenberg, N.M., K. Ravindran, and W.M. Kuebler, *TRPV4: physiological role and therapeutic potential in respiratory diseases.* Naunyn Schmiedebergs Arch Pharmacol, 2015. **388**(4): p. 421-36.

39. Vennekens, R., G. Owsianik, and B. Nilius, *Vanilliod Transient Receptor Potential Cation Channels: An Overview.* Current Pharmaceutical Design, 2008. **14**: p. 18-31.

40. Arniges, M., et al., *Swelling-activated Ca2+ entry via TRPV4 channel is defective in cystic fibrosis airway epithelia.* J Biol Chem, 2004. **279**(52): p. 54062-8.

41. Fernandez-Fernandez, J.M., et al., *Functional coupling of TRPV4 cationic channel and large conductance, calcium-dependent potassium channel in human bronchial epithelial cell lines.* Pflugers Arch, 2008. **457**(1): p. 149-59.

42. Earley, S., et al., *TRPV4 forms a novel Ca2+ signaling complex with ryanodine receptors and BKCa channels.* Circ Res, 2005. **97**(12): p. 1270-9.

43. Alvarez, D.F., et al., *Transient receptor potential vanilloid 4-mediated disruption of the alveolar septal barrier: a novel mechanism of acute lung injury.* Circ Res, 2006. **99**(9): p. 988-95.

44. Damann, N., et al., *The calcium-conducting ion channel transient receptor potential canonical 6 is involved in macrophage inflammatory protein-2-induced migration of mouse neutrophils.* Acta Physiol (Oxf), 2009. **195**(1): p. 3-11.

45. Hamanaka, K., et al., *TRPV4 channels augment macrophage activation and ventilator-induced lung injury.* Am J Physiol Lung Cell Mol Physiol, 2010. **299**(3): p. L353-62.

46. Hellwig, N., et al., *Homo- and heteromeric assembly of TRPV channel subunits.* J Cell Sci, 2005. **118**(Pt 5): p. 917-28.

47. Lorenzo, I.M., et al., *TRPV4 channel participates in receptor-operated calcium entry and and ciliary beat frequency regulation in mouse airway epithelial cells.* PNAS, 2008. **105**(34): p. 12611-12616.

48. Scheraga, R.G., et al., *TRPV4 Protects the Lung from Bacterial Pneumonia via MAPK Molecular Pathway Switching.* J Immunol, 2020. **204**(5): p. 1310-1321.

49. Simmons, S., et al., *Novel mechanisms regulating endothelial barrier function in the pulmonary microcirculation.* J Physiol, 2019. **597**(4): p. 997-1021.

50. Hamanaka, K., et al., *TRPV4 initiates the acute calcium-dependent permeability increase during ventilator-induced lung injury in isolated mouse lungs.* Am J Physiol Lung Cell Mol Physiol, 2007. **293**(4): p. L923-32.

51. Samapati, R., et al., *Lung endothelial Ca2+ and permeability response to platelet-activating factor is mediated by acid sphingomyelinase and transient receptor potential classical 6.* Am J Respir Crit Care Med, 2012. **185**(2): p. 160-70.

52. Yin, J., et al., *Role of transient receptor potential vanilloid 4 in neutrophil activation and acute lung injury.* American Journal of Respiratory Cell and Molecular Biology, 2015.

53. Balakrishna, S., et al., *TRPV4 inhibition counteracts edema and inflammation and improves pulmonary function and oxygen saturation in chemically induced acute lung injury.* Am J Physiol Lung Cell Mol Physiol, 2014. **307**(2): p. L158-72.

54. Achanta, S. and S.E. Jordt, *Transient receptor potential channels in pulmonary chemical injuries and as countermeasure targets.* Ann N Y Acad Sci, 2020. **1480**(1): p. 73-103.

55. Holmes, W.W., et al., *Conceptual approaches for treatment of phosgene inhalation-induced lung injury.* Toxicol Lett, 2016. **244**: p. 8-20.

56. Dietrich, A., M. Fahlbusch, and T. Gudermann, *Classical Transient Receptor Potential 1 (TRPC1): Channel or Channel Regulator?* Cells, 2014. **3**(4): p. 939-62.

57. Broker-Lai, J., et al., *Heteromeric channels formed by TRPC1, TRPC4 and TRPC5 define hippocampal synaptic transmission and working memory.* EMBO J, 2017. **36**(18): p. 2770-2789.

58. Clapham, D.E., *TRPC channels as cellular sensors.* Nature, 2003. **426**: p. 517-524.

59. Muraki, K., et al., *Na(+) entry through heteromeric TRPC4/C1 channels mediates (-)Englerin A-induced cytotoxicity in synovial sarcoma cells.* Sci Rep, 2017. **7**(1): p. 16988.

60. Cheung, S.Y., et al., *TRPC4/TRPC5 channels mediate adverse reaction to the cancer cell cytotoxic agent (-)-Englerin A.* Oncotarget, 2018. **9**: p. 29634-29643.

61. Carson, C., et al., *Englerin A Agonizes the TRPC4/C5 Cation Channels to Inhibit Tumor Cell Line Proliferation.* PLoS One, 2015. **10**(6): p. e0127498.

62. Vermeulen, V. *German Reference Centre for Ethics in the Life Sciences (2020): In Focus: Animal Experiments in Research*. 2006 21.03.2022]; Available from: http://www.drze.de/in-focus/animal-experiments-in-research.

63. Balcombe, J.P., N.D. Barnard, and C. Sandusky, *Laboratory Routines Cause Animal Stress.* American Journal for Laboratory Animal Science. **43**(6): p. 42-51.

64. Brooks, J., et al., *High Throughput and Highly Controllable Methods for In Vitro Intracellular Delivery.* Small, 2020. **16**(51): p. e2004917.

65. Huh, D., et al., *Reconstituting organ-level lung functions on a chip.* Science, 2010. **328**(5986): p. 1662-8.

66. Whitesides, G.M., *The origins and the future of microfluidics.* Nature, 2006. **442**(7101): p. 368-73.

67. Squires, T.M. and S.R. Quake, *Microfluidics: Fluid physics at the nanoliter scale.* Reviews of Modern Physics, 2005. **77**: p. 977-1026.

68. Stucki, A.O., et al., *A lung-on-a-chip array with an integrated bio-inspired respiration mechanism.* Lab Chip, 2015. **15**(5): p. 1302-10.

69. Blume, C., et al., *Temporal Monitoring of Differentiated Human Airway Epithelial Cells Using Microfluidics.* PLoS One, 2015. **10**(10): p. e0139872.

70. Humayun, M., C.W. Chow, and E.W.K. Young, *Microfluidic lung airway-on-a-chip with arrayable suspended gels for studying epithelial and smooth muscle cell interactions.* Lab Chip, 2018. **18**(9): p. 1298-1309.

71. Xu, Z., et al., *Application of a microfluidic chip-based 3D co-culture to test drug sensitivity for individualized treatment of lung cancer.* Biomaterials, 2013. **34**(16): p. 4109-4117.

72. Wu, Q., et al., *Organ-on-a-chip: recent breakthroughs and future prospects.* Biomed Eng Online, 2020. **19**(1): p. 9.

73. Uhlig, S. and O. Heiny, *Measuring the Weight of the Isolated Perfused Rat Lung During Negative Pressure Ventilation.* Journal of Pharmacological and Toxicological Methods, 1995. **33**: p. 147-152.

74. Uhlig, S. and L. Wollin, *An Improved Setup for the Isolated Perfused Rat Lung.* Journal of Pharmacological and Toxicological Methods, 1994. **31**(2): p. 85-94.

75. Krabbe, J., et al., *Retrograde perfusion in isolated perfused mouse lungs-Feasibility and effects on cytokine levels and pulmonary oedema formation.* Basic Clin Pharmacol Toxicol, 2019. **125**(3): p. 279-288.

76. von Bethmann, A.N.B., F.; Nüsing, R.; Vogt, K.; Volk, H.D.; Müller K-M.; Wendel, A.; Uhlig, S., *Hyperventilation Induces Release of Cytokines from Perfused Mouse Lung.* AMERICAN JOURNAL OF RESPIRATORY AND CRITICAL CARE MEDICINE, 1998. **157**: p. 263-272.

77. Weissmann, N., et al., *Activation of TRPC6 channels is essential for lung ischaemia-reperfusion induced oedema in mice.* Nat Commun, 2012. **3**: p. 649.

78. Norbert Weissmann*†, A.D., Beate Fuchs*, Hermann Kalwa‡, Mahmut Ay*, Rio Dumitrascu*,, U.S. Andrea Olschewski§, Michael Mederos y Schnitzler‡, Hossein Ardeschir Ghofrani*,, and O.P. Ralph Theo Schermuly*, Werner Seeger*, Friedrich Grimminger*, and Thomas Gudermann‡, *Classical transient receptor potential channel 6 (TRPC6) is essential for hypoxic pulmonary vasoconstriction and alveolar gas exchange.* PNAS, 2006. **103**.

Table of figures

Acknowledgements

With the submission of this thesis, my time at the WSI is ending and throughout the past years of this dissertation, I have received a lot of support and assistance.

Above all, I would like to express my gratitude to my primary supervisor, Alexander Dietrich, for his support and guidance in the past years. Your experience and expertise were invaluable for my research and brought my work to a higher level.

I would like to thank the head of the WSI and the GRK2338 - Targets in Toxicology, Thomas Gudermann, for the admission to the institute and enabling me to work on this project as well as the members of my TAK committee, Annette Nicke and Claudia Staab-Weijnitz.

Moreover, I would like to express my sincere thanks to both Julia and Steffi, the heart and soul of our GRK. Because of you and all the colleagues of the first cohort, the GRK was fun, educational and over far too soon.

I wish to extend my thanks to my colleagues from the Dietrich Lab. You made me feel welcome since the first day I set foot in the building, provided stimulating discussions and support. A special thanks to Jonas, who set the groundwork of my project and taught me everything about my cruel mistress.

I would like to acknowledge my former and current colleagues from the WSI as well, for their wonderful collaboration, the activities, the lunch and, more important, coffee breaks.

Finally, I could not have completed this dissertation without the support of my close friends, parents and family, who provided support and happy distractions for vital rest and peace of mind outside the institute.

And, of course, to Sara – for accepting me for who I am, for being there all the way through distance, stresses and moans. You have been amazing, I could not have done it without you!